(2)

FINAL TECHNICAL REPORT

for

HIGH CURRENT EXTRACTION IN THE STELLATRON

ONR Contract No. N00014-88-K-0175

October 1, 1987 - April 30, 1990

Principal Investigators

Norman Rostoker, Amnon Fisher and Hiroshi Ishizuka

Department of Physics

University of California

Irvine, California 92717

TABLE OF CONTENTS

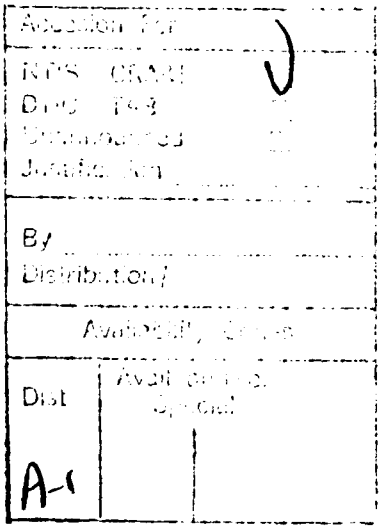

Experimental study of a stellatron accelerator using plasma start-up

H. Ishizuka
Department of Physics, University of California, Irvine, California 92717

(Received 5 March 1990; accepted 10 August 1990)

Formation and acceleration of a high-current electron beam in a stellatron were studied. The apparatus had a 41 cm major radius and 4 cm minor radius torus, which was pumped down to 10^{-7} Torr. Plasma was injected into the torus and confined in a rising stellarator field. A runaway current of up to a few kiloamperes was induced when applying the betatron field. Beams of over 1 kA and with a current density of approximately 1 kA/cm^2 were accelerated to several million electron volts with little loss. A 1 kA, 10 MeV beam was observed by initially forming a 2 kA beam. The loss was associated with negative-mass instability and high-mode orbital resonances.

I. INTRODUCTION

In the last three and a half decades there has been increased interest in generating a multi-kiloampere ring of energetic electrons. Pioneering work by Budker[1] on a space-charge neutralized ring was followed by extensive studies of the so-called plasma betatron.[2,3] A couple of plasma betatrons employed a stellarator field to confine the beam.[4,5] Non-neutral electron rings were also investigated with the intention of applying them in the Electron Ring Accelerator (ERA),[6] an ion accelerator. However, experimental results failed to meet theoretical expectations. In plasma betatrons the beam current was much smaller than the conduction current; termination usually occurred at an early stage of acceleration. Apparently, a difficulty lay in sustaining an equilibrium of these two currents simultaneously. Beam disruption was also caused by negative-mass instability[7] and two-stream instability.[4] Gas breakdown continued through the acceleration period and complicated the problem. In ERA investigations, acceleration of a 150 A beam from 3.3 to 18 MeV was reported.[8] However, in most cases electron rings collapsed as a result of negative-mass instability on the course of compression. Meanwhile, large runaway currents were observed in tokamaks[9] and stellarators[10] while attempting to heat a plasma. Energetic rings of up to 150 kA were achieved by relativistic electron beam (REB) injection, and the lifetime of a 60 kA ring reached 40 msec when the major radius was compressed.[11] Betatron acceleration of kiloampere REB rings in background plasma raised the beam energy from 1 to 3 MeV.[12] The relationship between single-particle acceleration and a large runaway current in a fusion device was discussed by Fessenden *et al.*[5]

Attention has recently been directed toward the use of a toroidal magnetic field to focus an intense electron beam in vacuum; a modified betatron[13,14] and a solenoidal lens betatron[15] have been under development. A stellatron[16,17] has a helical field together with the toroidal field for better control of the beam center. An experiment conducted at UC Irvine on the modified betatron showed that momentum mismatch resulting from the image charge set serious limits on the beam confinement.[18] In 1984 the device was converted to a stellatron.

After observing a 200 A beam using electron injection,[19] plasma start-up was introduced to increase the beam current to a kiloampere level.[20] Electron loss during acceleration was studied next.[21] Improvement in the field accuracy, and control of the orbit with time, led to a 1 kA beam at 10 MeV.[22] A fast shift of the orbit was utilized to measure the beam profile[23] and also to extract about 10% of the electrons from the torus.[24] In this paper we summarize the experimental results on beams that started from a plasma in high vacuum.

The theory of the stellatron has been developed by several authors.[16,17,25–31] In an $l=2$ stellatron, three types of magnetic fields are combined, as shown in Fig. 1: Vertical field,

$$B_v = B_{z0}(1 - nx/R); \tag{1}$$

toroidal field,

$$B_t = bB_{z0}[R/(R+x)]; \tag{2}$$

and rotating quadrupole field,

$$B_{hx} = \mu B_{z0}[(z\cos m\theta - x\sin m\theta)/R], \tag{3}$$

$$B_{hz} = \mu B_{z0}[(x\cos m\theta + z\sin m\theta)/R], \tag{4}$$

where θ is the angle in the toroidal direction. The motions of the beam center and each electron in this set of fields are determined analytically for $n=\frac{1}{2}$. The closed orbit of the beam is a helix,

$$\frac{x}{R} = (A\cos m\theta + \alpha)\frac{\Delta p}{p}, \quad \frac{z}{R} = A\sin m\theta\,\frac{\Delta p}{p}. \tag{5}$$

Here $\Delta p/p$ is the momentum error and α is the momentum compaction factor. As for a space-charge neutralized beam in a resistive torus, the self-field does not affect the motion of the beam center. Here b and μ are kept much larger than unity throughout the acceleration period ($\mu \lesssim b$ in the UCI stellatron). Under such conditions, A and α are given by

$$A = \mu/[\tfrac{1}{2}(m^2 + mb - \tfrac{1}{2}) + \mu^2], \tag{6}$$

$$\alpha = 1/[\tfrac{1}{2} + \mu^2(m^2 + mb - \tfrac{1}{2})^{-1}]. \tag{7}$$

 0899-8221/90/123149-12$02.00

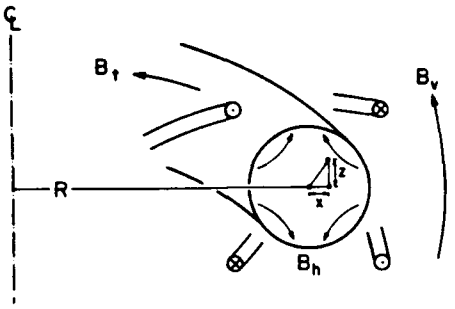

FIG. 1. Magnetic field configuration in a stellatron. A toroidal field B_t and a rotating quadrupole field B_h, produced by four helical windings, constitute a stellarator field for focusing an intense electron beam. A vertical field B_v is the betatron field that guides and accelerates the beam.

The beam center oscillates around the closed orbit mentioned above at the single-particle betatron tunes:

$$\omega_1 \approx b + m, \quad \omega_2 \approx -b, \qquad \omega_3 \approx \mu^2/mb(m+b), \quad \omega_4 \approx m; \tag{8}$$

each electron oscillates around the beam center. The self-magnetic field created by the electron motion within the beam provides additional focusing that can be of significant strength in actual experiments.[21,31]

If b changes during acceleration, ω_1 and ω_2 cross integers and half-integers successively and may cause beam loss. Negative-mass instability is also a serious problem because of its large growth rate. The longitudinal electron mass becomes negative above a transition energy, which, when the self-magnetic field of the beam is neglected, is approximately determined by

$$\gamma_{tr} \approx \mu/\sqrt{m(m+b)}. \tag{9}$$

Another instability is predicted that arises from the interaction between the quadrupole winding, a negative-energy transverse wave on the beam, and an electromagnetic waveguide mode.[30]

II. APPARATUS

During the course of the experiment the apparatus was modified; however, the dimensions of the torus were not changed. The schematic of the initial device is shown in Fig. 2. The latest configuration is illustrated in Fig. 3.

The torus was made of either glass or graphite–epoxy composite. The major and minor radii were 41 and 4 cm, respectively. The torus consisted of two half-tori so that they could be put in the toroidal coil system (which was also separable into two halves). The glass torus was either lined with stainless steel mesh or coated with molybdenum. Acceleration gaps were provided at the O-ring joints of the half-tori. A combination of a half glass torus and a half graphite torus was also used (Fig. 4). The torus was evacuated by a cryogenic pump down to 10^{-7} Torr.

The vertical field was produced by a pair of two-turn coils. In Fig. 2, an additional magnetic flux was provided by a center solenoid to satisfy the betatron condition. In the case of Fig. 3, inner loops supplied the magnetic flux

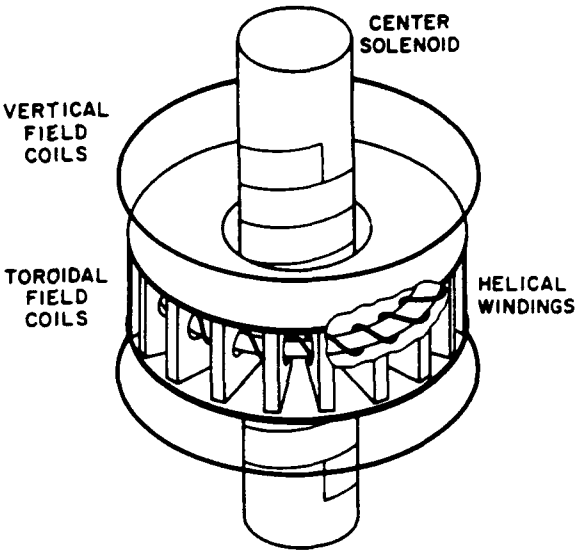

FIG. 2. Schematic of the original UCI stellatron.

instead of the center solenoid. The coils were activated by a 20 kV, 0.5 mF capacitor bank. The ratio of the electric current in the inner coils to that in the outer coils was not

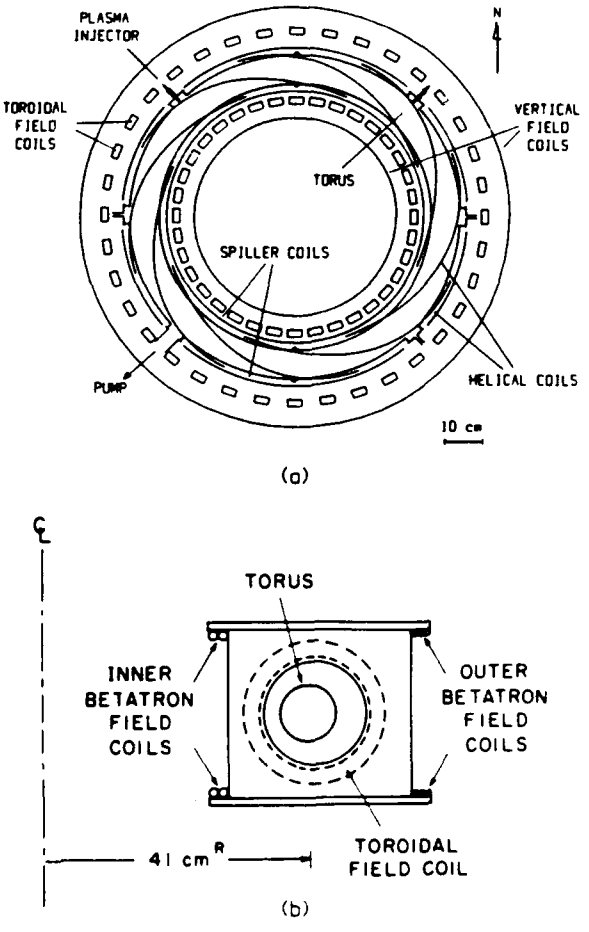

FIG. 3. The latest setup. (a) Top view. (b) Side view.

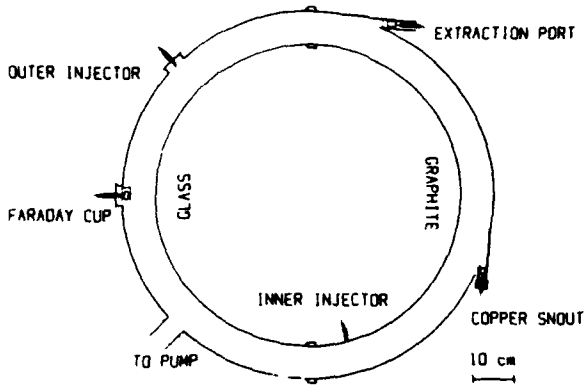

FIG. 4. Top view of the torus. In this example, a half-glass torus is combined with a half-graphite torus having tangential ports. In most cases, two half-glass tori are employed providing five ports to put in plasma injectors, probes, limiters, and/or x-ray targets.

TABLE I. Magnetic field parameters.

Vertical field:	
Peak field	Up to 1 kG on the minor axis
Field index	0–0.8 inside the torus
Rise time	60–100 μsec (0 to peak)
One-turn voltage	Up to 3 kV
Toroidal field:	
Peak field	Up to 17 kG on the minor axis
Rise time	70–120 μsec (0 to peak)
Rotating quadrupole field:	
Helical periods	0.5–6 around the torus
Rotational transform	Up to 0.25
Rise time	70–150 μsec (0 to peak)
Spiller field:	
Peak spiller current	Up to 6 kA
Rise time	≤1 μsec

normally kept constant, but was varied as a function of time by the use of inductors, capacitors, and resistors. In other words, the ratio of the field B on the minor axis of the torus to the average field $\langle B \rangle$ inside was programmed. A typical circuit is shown in Fig. 5.

The toroidal magnetic field was initially generated by 24 coils.[19] The azimuthal ripple was ±2% on the minor axis of the torus and ±8% at the outer wall of the torus. The ripple was reduced to 0.1% (calculated) on the minor axis and ±1% at the wall by increasing the number of coils to 36. The coil system was energized by a 20 kV, 1 mF capacitor bank. The $l = 2$ rotating quadrupole field was produced by four helical windings nested inside the toroidal field coils at 7.5 cm from the minor axis of the torus. The azimuthal mode number m was 12 initially, and then reduced to 8, 6, and 4. Later, m was changed from 4 to 3, 2, and 1 by placing the windings directly on the torus wall.

A fast-rising vertical field (referred to as the "spiller field" hereafter) was generated by one-turn loops wound on the inner and outer walls of the torus. This field was used to move the beam at an arbitrary time, and even to the torus wall, quickly. A current was fed from a 75 kV capacitor through a triggered spark gap. The spiller field normally opposed the betatron field, causing an expansion of the beam orbit.

The field parameters are listed in Table I.

A plasmoid was injected into the torus by a plasma gun (i.e., a 1/4 in. diam rigid coaxial cable). The power source was a 0.01–0.1 μF capacitor, charged at 3–10 kV and discharged through a hydrogen thyratron. A voltage pulse applied between the conductors produced a surface flashover at the end of the cable and projected a plasmoid. A small amount of neutral gas was released; although the torus was isolated from the pump by a gate valve (to test the plasma gun), the pressure did not increase by more than 10^{-5} Torr upon injection of the plasma.

III. BEAM FORMATION AND ACCELERATION

A time sequence of operation and typical signals at the early stage of the experiment are shown in Fig. 6. The 24

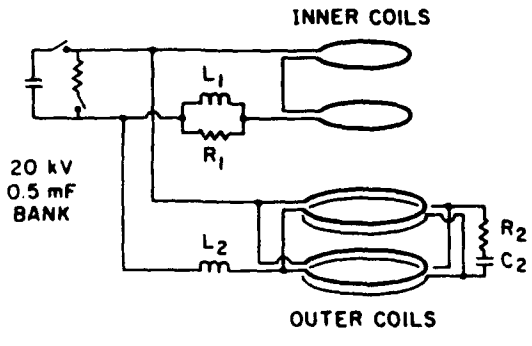

FIG. 5. Circuit to drive the betatron field coils. Electric currents in the inner and outer coils are programmed so that the beam position is controlled over time during acceleration.

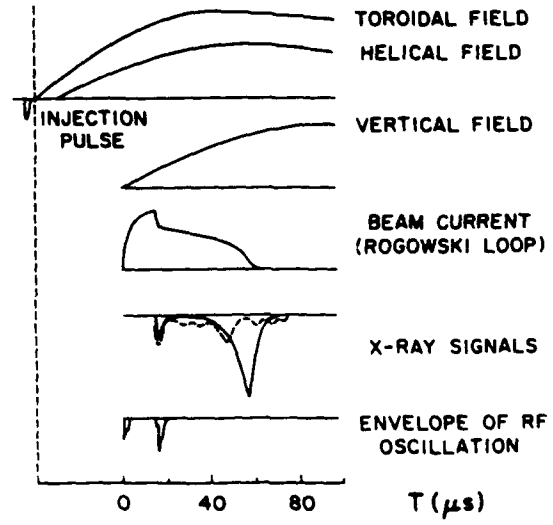

FIG. 6. Typical time sequence of operation and signals at the early stage of the experiment with the 24 toroidal coil system.

toroidal coil system was used; $\langle B \rangle / B$ was constant during a discharge. The plasma gun was fired a few microseconds before the start of the toroidal magnetic field, which was followed by the helical field in less than 10 μsec. The plasma was compressed in the x-z plane (as a result of the rising stellarator field), expanded around the major diameter of the torus, and formed a ring in approximately 20 μsec. The electron line density was varied up to 10^{12}/cm by changing the injection parameters. The vertical field, applied 40–60 μsec after the start of the toroidal field, generated a beam of runaway electrons. Strong rf activity was detected for the first few microseconds. The frequency spectrum, measured with bandpass filters, covered 200 MHz to over 1.5 GHz, and suggested the occurrence of turbulence originating from the beam–plasma interaction. No beam was formed if either the toroidal, helical, or betatron field was absent. The minimal rotational transform angle, $\iota/2\pi$, to observe the beam was approximately 0.03.

Weak beams of less than 200 A, generated by means of plasma start-up, behave in a similar way to those formed by electron injection. Even at much higher currents no phenomenon appears that is totally new, except for rf oscillations at the beginning of beam formation. Based on these observations, instabilities related to plasmas are not important during acceleration.

The beam current I_b increased with time and reached a plateau as the electrons gained velocity and became relativistic. At this time a Rogowski loop showed a sudden drop of the beam current. Accompanying this were bursts of rf oscillations and x rays. The disruption was clear for beams of over 500 A and became more pronounced as the original beam current was increased. Thus the current after the disruption was not necessarily an increasing function of the peak current, but was maximized by restraining the peak current properly. For example, a current of 1 kA outlived the disruption when the peak current was about 1.3 kA, while a current of a few hundred amperes remained out of a 3 kA peak current.

Beam electrons that survived the early disruption were gradually lost. The x-ray signals showed successive small peaks. The beam was terminated when the ratio of the toroidal field to the vertical field decreased to $B_t/B_v = 24 - m$. The x rays attained the maximum intensity at this time. Collimated x-ray detectors revealed that electrons hit the torus wall at m spots separated equally around the major diameter. The torus wall flashed as a result of electron bombardment at these spots. The flash was bright enough to be photographed with an open-shutter camera under normal room lighting conditions. Pictures showed that the beam took a helical orbit (Fig. 7), in agreement with theory. The x-ray pinhole pictures displayed m thin arcs that extended along the helical windings, each corresponding to the core of the bright spot in the optical picture [see Fig. 19(b)]. The rf oscillations were not detected after the early disruption.

The beam lifetime was prolonged by increasing the strength of the toroidal field and setting $\langle B \rangle / B$ at 2.2–2.3 on the minor axis of the torus. The peak electron energy exceeded 11 MeV when the toroidal magnetic field

FIG. 7. Open-shutter picture of the torus flashing as a result of electron bombardment. The beam dumped to the torus wall causes m bright arcs equally separated around the major diameter of the torus. One of them is seen here.

was increased to 15 kG (Fig. 8). The beam energy was evaluated using the equation $dp/dt = e(V_{\text{loop}} - L\, dI_b/dt)/2\pi r$. Here V_{loop} is the loop voltage at a radius r and L is the self-inductance of the beam. Here V_{loop} was measured on the minor axis of the torus, and was usually monitored at the outer wall of the torus when operating the machine. Values of V_{loop}/r at these positions were equal to each other within 1% under normal operating conditions. Here L was calculated, assuming a ring whose major and minor radii were 41 and 0.5 cm, respectively. (Error in the calculated beam energy resulting from the discrepancy between this assumption and the real beam dimension is less than 1% at energies above a few mega-electron-volts.) The calculated beam energy was checked experimentally by means of the electron absorption method.[24]

The whole current was carried by runaway electrons. This was verified as follows: first, the ratio of the x-ray intensity to the beam current was the same for both the electron injection and plasma start-up; second, regarding the beams started from plasma, the x-ray intensity was proportional to the beam current over a wide range. The beam was dumped onto a target by applying the spiller field at different energies during acceleration. In Fig. 9 the

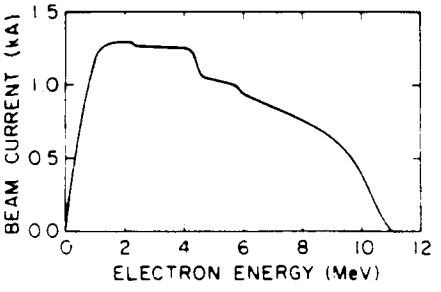

FIG. 8. Beam current versus energy for a high-field discharge with the 24 toroidal coil system. Here B = 15 kG.

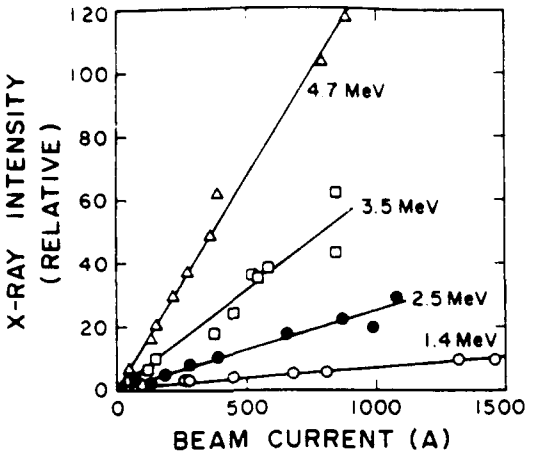

FIG. 9. The x-ray yield versus beam current. The beam is spilled to a target at designated energies (±0.1 MeV) on the course of acceleration.

x-ray signal (from a PIN diode aimed at the target) is plotted against the beam current at the spill time.

The beam current never again increased once it reached a plateau. About 10% of the accelerated charge was extracted through a tangential port, while most of the beam hit a snout. An unbiased Faraday cup, oppositely directed to the electron beam, detected ions.[24] These observations support the view that the current was carried by runaway electrons while ions were confined within the beam. The effect of background gas on the beam was seen if the base pressure was made higher than 10^{-5} Torr: the peak current became larger but the beam disrupted, as in the case where too much plasma was injected.

IV. BEAM LOSS AND ITS SUPPRESSION

As mentioned in Sec. III, two distinct types of losses caused reduction of the beam current. One of them occurred abruptly at an early stage of acceleration. The other was gradual and eventually terminated the beam. Modifications of the apparatus were made in increments, with repeated scan of the operation parameters, to improve the beam confinement.

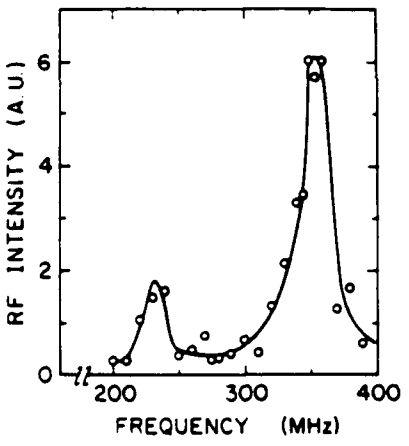

FIG. 10. rf spectrum at second and third harmonics during the early disruption, measured by a bandpass filter with a 5% resolution.

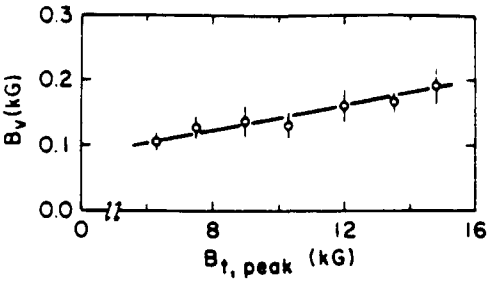

FIG. 11. The vertical field at the first beam disruption as a function of the toroidal magnetic field.

A. Early disruption

The first notable loss occurred when the beam energy was 0.7–2 MeV. A slight decline of the beam current was observed when the beam current was at the 100 A level. This decline became evident as the beam current was increased. Often the decay happened in a few steps [specifically, when the toroidal magnetic field was strong and the beam loss at the first step was slight (Fig. 8)]. The spectrum of the rf oscillations peaked at harmonics of the gyration frequency for motion of relativistic electrons around the major diameter of the torus. The fundamental mode, observed directly with a synchroscope, showed that the amplitude was irregularly modulated. Jumps in the phase were also seen sporadically. Figure 10 shows the second and third harmonics measured with bandpass filters. When the beam disruption was violent a fluorescent bulb, placed within about 0.5 m from the torus, illuminated, signaling the generation of intense rf emission. The disruption was delayed as the toroidal magnetic field was increased (Fig. 11). The beam current (immediately after the disruption) versus the rotational transform angle is shown in Fig. 12. Here the shaded area indicates a domain where the data points for a peak toroidal field of 14.4 kG are distributed. The fluctuation in the data was caused by the strong dependence of the disruption on the beam current, which was especially sensitive above 1 kA. The current that outlived

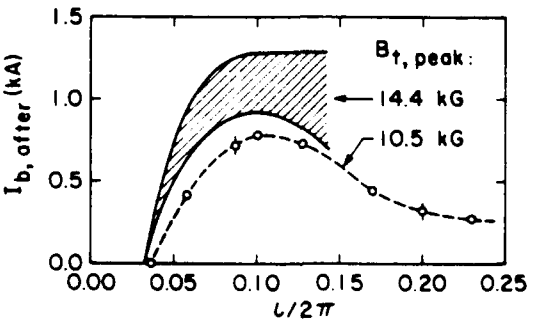

FIG. 12. Beam currents immediately after the first disruption versus the rotational transform angle.

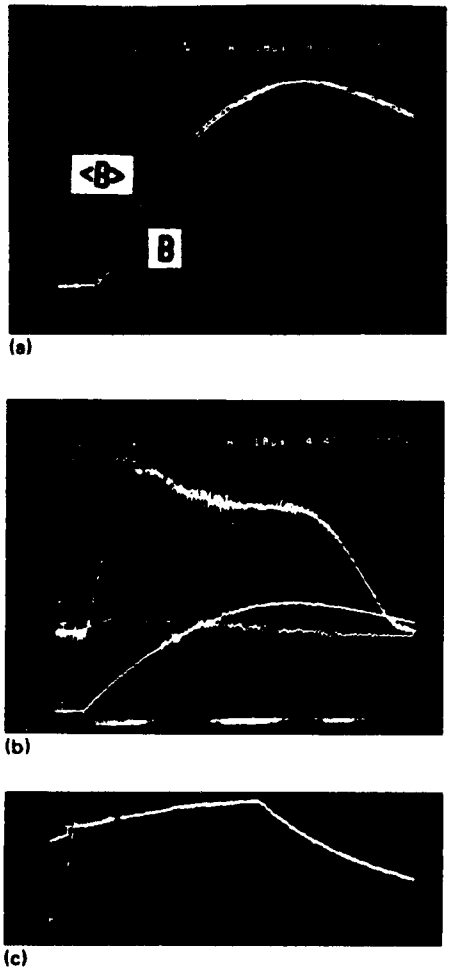

FIG. 13. Suppression of the early disruption by orbit control. (a) Vertical field B on the minor axis of the torus and the average field $\langle B\rangle$ inside (normalized). The peak beam energy is 4 MeV. (b) Beam current 322 A/div. (c) Helical coil current, cut down near the peak of the vertical field to reduce the magnetic force. The number of toroidal field coils is 36.

the disruption was peaked around $\iota/2\pi = 0.1$. It should be noted that the best beams were always observed under this condition, independent of the mode number m.

The disruption was not mitigated by changing the number of the toroidal field coils from 24 to 36, but was relieved by programming the betatron field so that the beam orbit was maintained close to the torus wall or a limiter. The temporal control of the orbit was accomplished by adjusting the circuit parameters in Fig. 5. The resistor R_1 advanced the phase of the current flowing in the inner betatron field coils. Here R_1 was altered in increments of 0.05 Ω, up to a maximum of 0.5 Ω. In addition, R_2 and C_2 delayed the phase of the current in the outer betatron field coils. The beam was located through the detection of x rays with collimated detectors. The beam stayed near the outer wall of the torus when $\langle B\rangle/B$ was made significantly larger than 2 at the initial stage of acceleration and decreased afterward. Figure 13(a) compares waveforms of $\langle B\rangle$ and B that produced the beam current shown in Fig. 13(b). Here $\langle B\rangle/B$ at the peak field

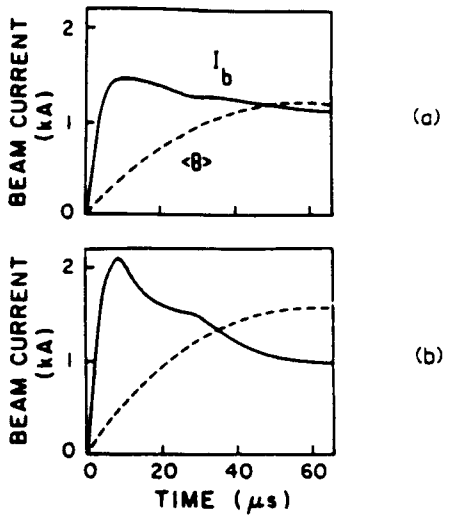

FIG. 14. Temporal change of the beam current for peak energies of (a) 5.5 MeV and (b) 7 MeV. The electron loss during acceleration becomes heavier as the peak energy is increased.

was 2.25. A sharp drop of the beam current as in Fig. 6 is not seen here. There were 36 toroidal field coils in this case.

Figure 14 shows the beam current as a function of time for different peak energies. The operation parameters were adjusted to observe a beam current larger than 1 kA at the peak of the betatron field. Note that an abrupt loss was avoided for peak energies of up to several mega-electronvolts. As the peak energy was further increased, ranges of the operation parameters narrowed and losses at the initial stage of acceleration became inevitable. Here 10 MeV, 1 kA beams were obtained when a 2 kA beam was initially formed (Fig. 15).

B. Gradual decay and termination

With the 24 toroidal coil system, the Rogowski loop showed a gradual decay of the beam that was insensitive to

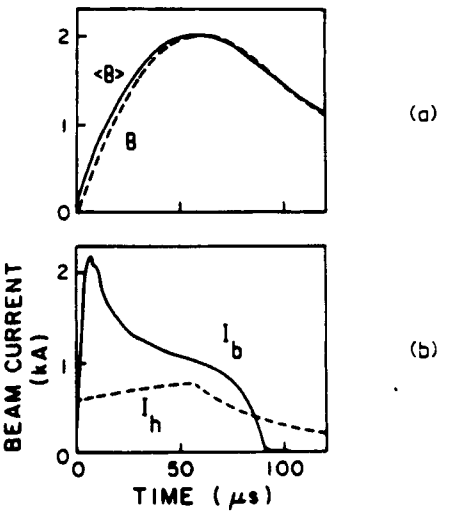

FIG. 15. Typical 1 kA, 10 MeV beam current. (a) Normalized $\langle B\rangle$ and B. (b) Beam current and helical current.

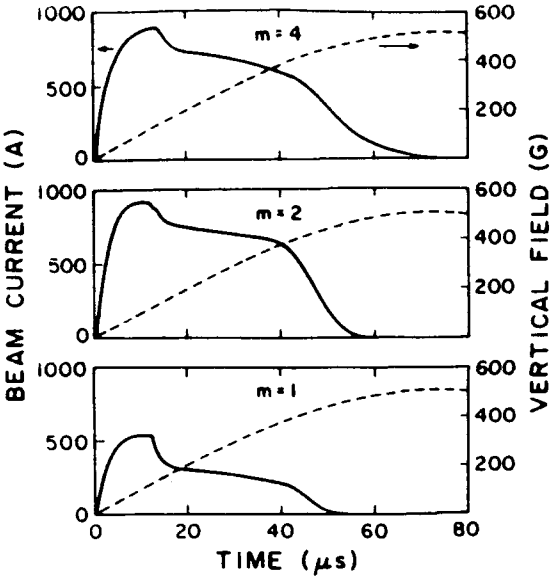

FIG. 16. Beam current waveforms for different helical mode numbers. The lifetime becomes shorter as m is reduced, while the current is nearly the same for $m \neq 2$. The number of toroidal field coils is 24 and $B_t = 10.5$ kG. The beam termination is eliminated by reducing the spatial ripple of the toroidal field using 36 coils.

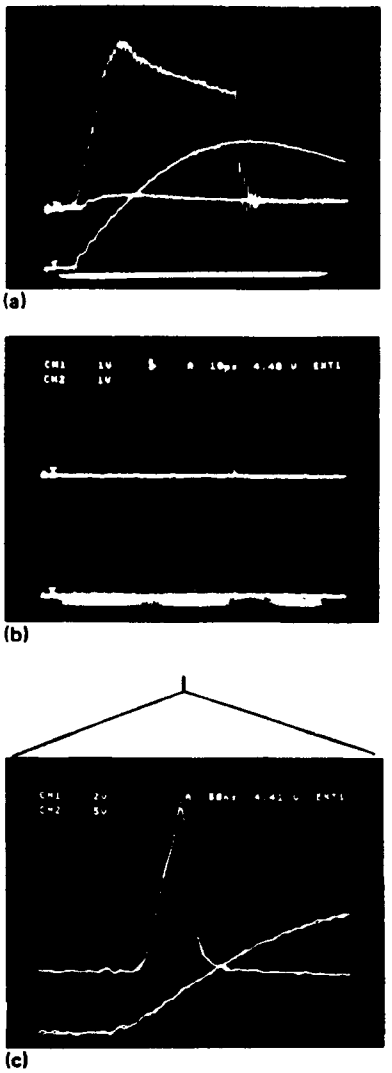

FIG. 17. Fast expansion of the beam orbit. (a) Upper trace: beam current, 322 A/div. Lower trace: betatron flux. (b) The x-ray signal from a PIN diode aimed at the west target (upper trace) and southeast target (lower trace). Sweep: 10 μsec/div. (c) Upper trace: x-ray waveform. Lower trace: spiller current. Sweep: 50 nsec/div.

the current. Collimated x-ray detectors aimed at major sources of x rays produced continuous signals corresponding to the decrease of the beam current. On the other hand, detectors looking at other portions of the torus presented small peaks during the decay (Fig. 6). When the strength of the toroidal field was changed, these peaks shifted in such a manner that the ratio of the vertical field to the toroidal field was conserved.

The beam eventually terminated, generating a large peak in the x-ray signal. The termination was not caused by momentum mismatch as a 10% shift of $\langle B \rangle / B$ had little effect on the beam's lifetime. The strength of the helical field also had little effect; however, the x-ray peak became more or less broader as the helical field was increased. The final disruption was influenced by the strength of the toroidal field and the azimuthal mode number m of the helical field. The beam endured a higher vertical field when the toroidal magnetic field was increased. The beam ended at a lower vertical field if m was reduced (Fig. 16). The quantity $(24 - m)$ described the ratio of the toroidal field to the vertical field at the time of beam extinction when there were 24 toroidal field coils. The gradual decay of the beam was greatly reduced and the termination of the beam was fully eliminated when the 36 toroidal coil system was used. As seen in Figs. 13 and 15, the current vanished after the helical field was diminished.

V. BEAM PROFILE

A quick shift of the orbit was applied to measure the minor dimension of the beam. The beam was swept to intercept two targets; electrons progressively scraped off of these targets were detected through x rays. Unlike the two probe method,[12] both targets were placed outside of the minor axis of the torus in this experiment. The targets were brass plates, which were 4 cm high, 6 mm wide, and 1/8 in. thick. One of them was placed at the west port and the other at the southeast port [Fig. 3(a)]. The spiller windings were put on the torus wall close to the median plane, and the outer windings were steered clear of the ports. A current was fed from a 0.05 μF capacitor charged up to 60 kV through a triggered spark gap.

The west target was fixed in such a way that the front was at 18 mm from the outer wall of the torus. It served as a limiter and also as a source of x rays for monitoring the beam. The southeast target was moved radially. The 36 toroidal coil system with $m = 4$ helical coils was used, and the beam parameters were 5 MeV and 0.9–1.1 kA.

The beam was spilled at the peak of the betatron field [Fig. 17(a)]. Here x rays from each target were detected by PIN diodes [Fig. 17(b)], giving rise to triangular signals [Fig. 17(c)]. The rise time of the signal was longer than the

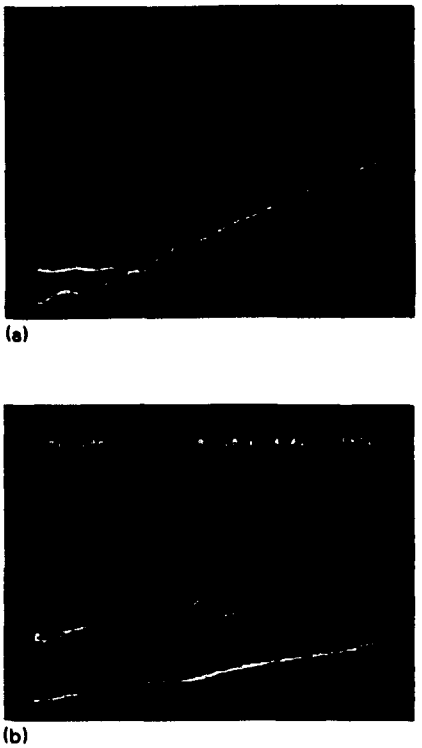

FIG. 18. (a) The x rays from the southeast target set at different radial positions. The largest signal is for the standard position. The middle and the smallest are for 0.5 and 2 mm outside, respectively. Sweep: 20 nsec/div. (b) Initial part of the x-ray signal. The target is moved at an interval of 1 mm. Sweep: 10 nsec/div. The lower traces are the spiller current.

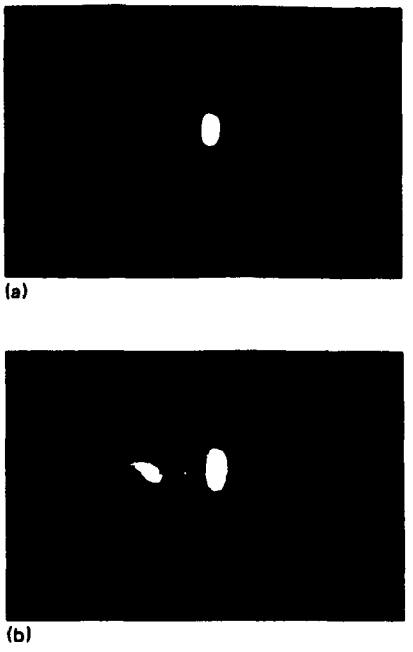

FIG. 19. The x-ray pinhole pictures of thin wires extending vertically. Two wires are arranged at 10 and 5 mm from the outer wall of the torus. (a) The beam hits the inner wire. (b) Electrons cross the outer wire (middle spot) and reach the torus wall (left spot) when the spiller field is applied.

decay time for $dI_{sp}/dt > 6$ kA/μsec. Here I_{sp} is the spiller current. When dI_{sp}/dt was reduced, the x-ray signal became broader and the decay was particularly prolonged. Modulations in the spiller current produced correlated modulations of the x-ray signal.

The standard position of the southeast target was chosen so that the x-ray signals from both targets had the same intensity. The x-ray signal decreased at the southeast target and increased at the west target as the southeast target was moved outward. Figure 18(a) shows x-ray signals for different target positions. The start of the x-ray signal was delayed as the target was moved outward. In Fig. 18(b), the southeast target was moved from the standard position by 1 mm; at the same time the PIN diode was moved closer to the port so that the x-ray signals at the beginning had nearly the same form. The expansion speed of the beam orbit determined in this way was 0.11 mm/nsec for $dI_{sp}/dt = 10$ kA/μsec, and changed in proportion to dI_{sp}/dt. The distribution of the electron density was derived from the waveform of the x-ray signal, as discussed in the next section.

A rough check of the beam size was performed by taking x-ray pinhole pictures of the movable target. Thin tungsten wires arranged vertically at different radii were also used for the same purpose. Most electrons, if not all, hit the inner wire during normal operation [Fig. 19(a)]. When the spiller field was applied a section of the outer wire [the middle spot in Fig. 19(b)] appeared in the picture along with a spot in the torus wall [the left image in Fig. 19(b)]. Apparently, the beam went across the tungsten wires and reached the outer wall of the torus. Measurements of the heights of these new images implied that the beam was less than 1 cm in diameter.

VI. DISCUSSION

A. Plasma start-up

The plasma, produced by flashover on a Teflon surface, contains carbon and fluorine ions that are not necessarily singly charged.[33] For the sake of simplicity, however, we assume a carbon plasma and also assume that the plasma expands around the torus at the ion sound velocity. Adiabatic compression resulting from the rising stellarator field heats the plasma. As plasma is detected on the opposite side of the torus ~ 20 μsec after the start of the toroidal field, the electron temperature is of the order of 500 eV.

The critical electric field E_c for runaway to occur is given by[34,35]

$$E_c = 5.2 \times 10^{-12} (n/T) \text{ V/cm}, \tag{10}$$

where n is the plasma density in cm^{-3} and T is the electron temperature in electron volts. The electron line density that gives rise to a 1 kA relativistic beam is 2.1×10^{11}/cm. The critical field is less than 10 mV/cm, even if the minor cross section of the plasma is as small as 1/4 cm^2. In the present experiment the toroidal electric field at

the time of beam formation is typically 5–10 V/cm, which is strong enough to drive all the plasma electrons into the runaway mode.

B. Loss of electrons

1. Early disruption

The loss is severe when the original beam current is high. Obviously, a collective instability is responsible for this disruption. Strong rf oscillations at harmonics of the electron gyration frequency around the torus, and also the beam energy at which the disruption occurs, point to negative-mass instability. The observed energies agree with (9) in order of magnitude, but are not consistent in their dependences on B_t and B_h. It must be noted that (9) applies only to a non-neutral beam. In the neutralized case, transverse focusing by the self-magnetic field boosts the threshold energy and reduces the growth rate.[31] The efficiency increases with increasing beam current density. The experimental dependence of the beam energy on the toroidal magnetic field (Fig. 11) is attributed to the minor-radius compression of the beam by the toroidal magnetic field.

The Kruskal–Shafranov limit is another suspect that may cause the disruption. However, kiloampere beams do not suffer loss if the energy is kept low.[21] Negative-mass instability is more consistent with experiments that clearly indicate the existence of an energy threshold. An electromagnetic instability characteristic of a quadrupole-focusing accelerator[30] may be ruled out since the observed disruption is insensitive to the mode number m.

2. Gradual decay

The slow loss is attributed to single-particle orbital instabilities. Though the beam current seems to decrease smoothly, small bursts of x rays occur intermittently (Fig. 6). During acceleration the beam encounters many integer and half-integer resonances (as frequently as ~ten resonances per microsecond). The result should be a diffusive loss of electrons, yet some resonances can cause sudden spills that are detectable only through x-ray emissions.

3. Final disruption

The beam is terminated at a certain value of b, the ratio between the toroidal field and the vertical field. Significant dependence on the beam current is not seen. This means that the final collapse is caused by a single-particle process. As mentioned before, the beam's lifetime is insensitive to a moderate change in $\langle B\rangle/B$. This is reasonable, as the machine was operated at a rotational transform angle $\iota/2\pi \simeq 0.1$, which allowed momentum errors greater than 10% when the oscillatory motion of electrons is taken into account. The value of b at the time of beam extinction is given by $24 - m$ when the 24 toroidal coil system was used. This indicates that the spatial ripple of the toroidal magnetic field causes the resonant loss of electrons.[26] The present experiment shows that the ripple must be smaller than 1% if the resonant loss is not to be serious.

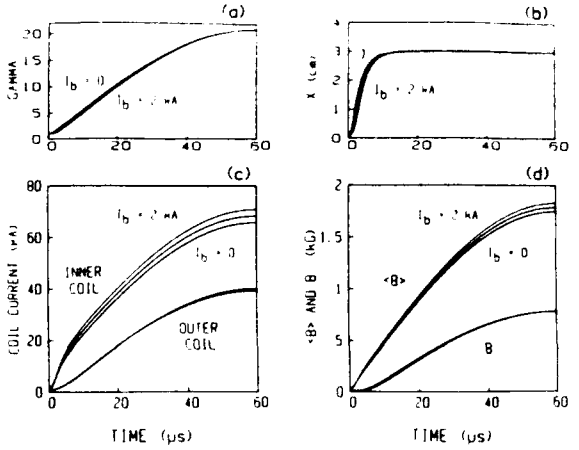

FIG. 20. Orbit control. The beam position converges from $x = 0$ to $x = 3$ cm exponentially with the beam energy γ. (a) γ. (b) Beam position. (c) Currents in the inner and outer loops causing the above shift. (d) The vertical field on the minor axis of the torus and the average field inside. Here $B_t = 15$ kG, $m = 4$, and $\iota/2\pi = 0.1$.

C. Orbit control

Let us consider how to program the currents in vertical field coils to have the beam position $\overline{x}$, averaged over θ, change as a given function of beam energy. The vector potential $A^{\rm ext}$ at $\overline{x}$ as a result of the coil current is determined as a sum of the electron momentum and the vector potential $A^{\rm self}$ resulting from the beam current. The field strength B on the torus minor axis is also determined by the use of Eqs. (5) and (7). Parameters include the toroidal magnetic field, helical field, beam current I_b at the final energy, and the beam minor radius. Electric currents in the inner and outer loops are calculated so as to give the above $A^{\rm ext}$ and B. Thus $\overline{x}$, the current $I^{\rm in}$ in the inner coil, the current $I^{\rm out}$ in the outer coil, and, accordingly, the magnetic field at an arbitrary position are correlated with each other through the beam energy. If we specify the time dependence of one of these and assign the final beam energy, then all the quantities can be expressed as functions of time.

Examples are shown in Fig. 20. Here, a beam, having a 5 mm minor radius and initially located at $\overline{x} = 0$, converges exponentially with γ to $\overline{x} = 3$ cm at a rate such that $\overline{x} = 2.7$ cm at 1.5 MeV. The geometric mean of $I^{\rm in}/I^{\rm in}_{\rm max}$ and $I^{\rm out}/I^{\rm out}_{\rm max}$ was assigned the value $\sin(\pi t/2T_{1/4})$ to simulate the circuit shown in Fig. 5. The coil currents and the field strength derived here are in close agreement with experimental values. In Fig. 20(d), $\langle B\rangle$ is the average field inside the torus minor axis. It is seen that $\langle B\rangle/B$ at the peak field is approximately 2.2 for $I_h = 0$ and above 2.3 for $I_h = 2$ kA. In the experiment, the peak of B is delayed by several microseconds from that of $\langle B\rangle$ [Fig. 13(a)]. The effect of this is that the beam, remaining at nearly a constant radius, begins to shrink as B approaches its peak. This may explain the observation that the beam is not lost even if the helical current is reduced at the later stage of acceleration [Figs. 13(b) and 13(c)].

The spiller field changes the major radius of the beam more quickly. The speed is roughly estimated as follows:

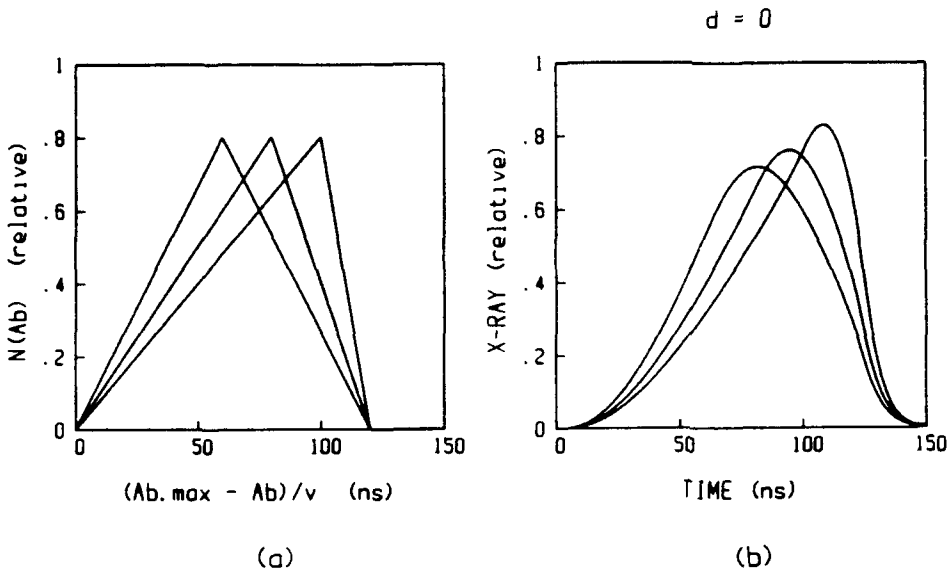

FIG. 21. (a) Electron distributions as functions of betatron amplitude. (b) Corresponding x-ray waveforms.

the momentum error caused by the spiller field drives the beam center, while the momentum compaction gives rise to a restoring force. The radial motion of the beam center from the original position $\bar{x}_i$ is then subject to the force

$$\frac{d^2\bar{x}}{dt^2} \approx \frac{ec\beta B_{sp}}{m_0\gamma} - \frac{1}{\alpha}\left(\frac{c}{R+\bar{x}_i}\right)^2(\bar{x}-\bar{x}_i), \tag{11}$$

where m_0 is the electron mass and B_{sp} is the spiller field. When the spiller field is applied, the orbit radius starts to change at a rate proportional to dB_{sp}/dt and inversely proportional to the momentum compaction factor. A damped oscillation is superimposed on it. For the parameters of the spiller windings in Sec. V and for $dI_{sp}/dt = 10$ kA/μsec, (11) predicts a velocity of 0.15 mm/nsec at the early stage of orbit expansion, about 40% higher than measured.

D. Beam profile

The density profile of a circulating beam is determined by the spread in betatron amplitude and by the spread in momentum. With targets located only outside of the original orbit, the density profile can be obtained when one of these spreads dominates. The observation that the x-ray signal changed its shape with dI_{sp}/dt suggests that the spread in the betatron amplitude is dominant; the betatron oscillation can grow during orbit expansion as a result of the asymmetry of the spiller field but the momentum distribution should not change significantly.

Let us introduce the following notation: A_b for the betatron amplitude, $N(A_b)$ for the electron distribution in the betatron amplitude, r for the distance from the minor axis of the beam, R_c for the major radius of the beam center, and R_t for the radial position of the target. The electron density $n(r)$ is given by $N(r)/2\pi r$. When the beam orbit expands electrons having A_b larger than $R_t - R_c$ get a chance to hit the target. The probability for the electron to be at a radial position $R > R_t$ is given by $P(R > R_t) = \cos^{-1}[(R_t - R_c)/A_b]/\pi$. In one gyration period, t_g, around the torus $P(R > R_t) \propto N(A_b)$ is taken by the target. If the expansion velocity is v and electrons are intercepted by two targets then $N(A_b)$ changes with time as

$$\frac{dN(A_b)}{dt} = -\frac{N(A_b)}{\pi t_g}\left[u(t-t_1)\cdot\cos^{-1}\left(1-v\frac{t-t_1}{A_b}\right) + u(t-t_2)\cdot\cos^{-1}\left(1-v\frac{t-t_2}{A_b}\right)\right], \tag{12}$$

where $t_1 = (A_{b,\max} - A_b)/v$ and $t_2 = (A_{b,\max} + d - A_b)/v$, d being the radial position of the second target measured from the normal position. Here $u(x)$ is the unit step function and t is measured from the instant when the outer edge of the beam comes into contact with the first target. The first and second terms on the right-hand side of Eq. (12) are proportional to the x-ray intensity from the first and second targets, respectively. Equation (12) is solved analytically, and the x-ray signals from the two targets are calculated if $N(A_b)$ is given. Figure 21 shows test distributions and corresponding x-ray signals for $d = 0$. Here $A_{b,\max}/v$ is 120 nsec. Let us note that the curves in Fig. 21(b) bear resemblance to previous x-ray signals observed (Figs. 17 and 18).

Attempts were made to extract $N(A_b)$ from the x-ray waveform.[23] One method is illustrated in Fig. 22. The downward curve of the x-ray signal is modified, as shown by the dotted line in Fig. 22(a). Here $n(r) = X(t)/v(t_e - t)$ is plotted in Fig. 22(b), where $X(t)$ is the x-ray intensity at time t. Taking into account the possible growth of the betatron oscillation during orbit expansion, and also the apparent increase of the width as a result of oscillatory movement of the beam, one may assume that the above evaluation gave the upper limit of the radius. The 1 kA current and density distributions as in Fig. 22(b) give current densities in excess of 1 kA/cm^2 around the beam axis.

Although the experimental result agreed with theory as a whole, some questions still remain unanswered. For example, it is not yet understood why the abrupt loss is suppressed when the beam touches a limiter. Also it is not

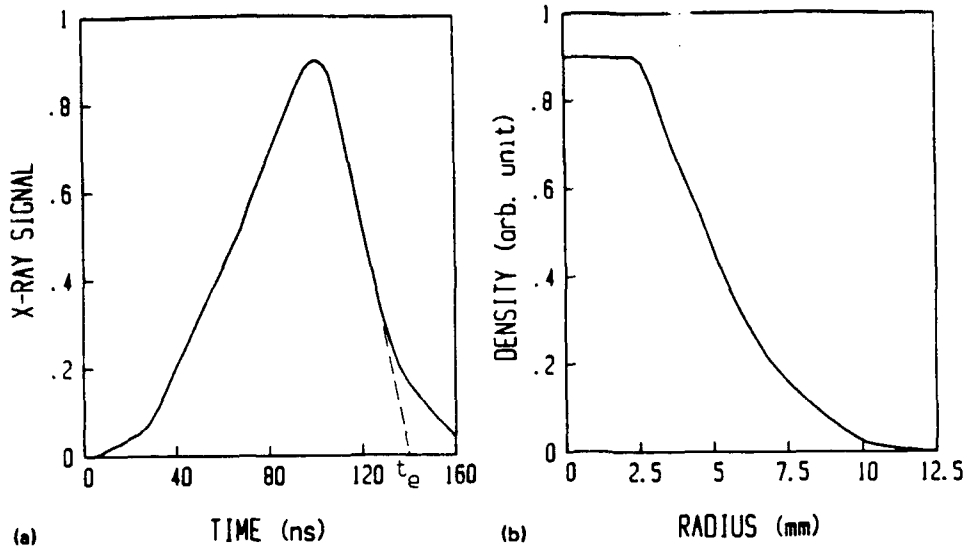

FIG. 22. (a) The x-ray signal for an expansion velocity of 0.082 mm/nsec. (b) Corresponding electron density profile.

known why $\iota/2\pi \simeq 0.1$ is the optimal transform angle. Recently, rotating quadrupole windings were added to the NRL modified betatron, and beam accelerations of up to 12 MeV were observed.[36] The apparatus is different from the UCI stellatron in size, injection scheme, and other aspects. Future understanding of stellatron performance will be deepened by experimental data from these machines.

ACKNOWLEDGMENTS

The author is indebted to B. Mandelbaum who participated in the early part of the work and R. Prohaska for technical assistance. Careful revision of the manuscript by K. Yee is gratefully acknowledged.

This work was supported by the Office of Naval Research and done in collaboration with N. Rostoker and A. Fisher.

[1] G. I. Budker, in *Proceedings of CERN Symposium on High-Energy Accelerators and Pion Physics*, Geneva, 1956 (CERN Scientific Information Service, Geneva, 1956), Vol. 1, p. 68.
[2] P. Reynolds and M. M. Skarsgard, J. Nucl. Energy C: Plasma Phys. **1**, 36 (1959).
[3] L. A. Ferrari and K. C. Rogers, Phys. Fluids **10**, 1319 (1967).
[4] K. Yatsu, Jpn. J. Appl. Phys. **8**, 606 (1969).
[5] See AIP Document No. PAPS-PFBPE-02-3149-21 for 21 pages of "Preliminary Study of the Acceleration of Electrons in a Plasma Betatron," UCRL-78014 by T. Fessenden, C. W. Hartman, and R. H. Munger (1976). Order by PAPS number and journal reference from American Institute of Physics, Physics Auxiliary Publication Service, 335 East 45th Street, New York, NY 10017. The price is $1.50 for each microfiche (98 pages) or $5.00 for photocopies of up to 30 pages, and $0.15 for each additional page over 30 pages. Airmail additional. Make checks payable to the American Institute of Physics.
[6] V. I. Veksler, V. P. Sarantsev, A. G. Bonchosmolovsky, G. V. Dolbilov, G. A. Ivanov, I. N. Ivanov, M. L. Iovnovich, I. V. Kozhukhov, S. B. Kusnetsov, V. G. Makhan'kov, E. A. Perel'shtein, V. P. Rashevsky, K. A. Reshetnikova, N. B. Rubin, S. B. Rubin, P. I. Ryl'tsev, and O. I. Yarkovov, in *Collective Methods of Acceleration*, edited by N. Rostoker and M. Reiser (Harwood Academic, New York, 1979), p. 23.
[7] L. A. Ferrari, K. C. Rogers, and R. W. Landau, Phys. Fluids **11**, 691 (1968).
[8] D. Keefe, G. R. Lambertson, L. J. Laslett, W. A. Perkins, J. M. Peterson, A. M. Sessler, R. W. Allison, Jr., W. W. Chupp, A. U. Luccio, and J. B. Rechen, Phys. Rev. Lett. **22**, 558 (1969).
[9] H. Knoepfel, D. A. Spong, and S. J. Zweben, Phys. Fluids **20**, 511 (1977).
[10] K. M. Young, Plasma Phys. **16**, 119 (1974).
[11] A. Mohri, Nucl. Fusion **25**, 1299 (1985).
[12] D. Taggart, M. R. Parker, H. Hopman, and H. H. Fleischman, IEEE Trans. Nucl. Sci. **NS-30**, 3165 (1983).
[13] P. Sprangle and C. A. Kapetanakos, J. Appl. Phys. **49**, 1 (1978).
[14] N. Rostoker, Comments Plasma Phys. **6**, 91 (1980).
[15] S. Humphries, Jr. and D. M. Woodall, Bull. Am. Phys. Soc. **28**, 1054 (1983).
[16] C. W. Roberson, M. Mondelli, and D. Chernin, Phys. Rev. Lett. **50**, 507 (1983).
[17] C. W. Roberson, M. Mondelli, and D. Chernin, Part. Accel. **17**, 79 (1985).
[18] H. Ishizuka, G. Lindley, B. Mandelbaum, A. Fisher, and N. Rostoker, Phys. Rev. Lett. **53**, 266 (1984).
[19] B. Mandelbaum, H. Ishizuka, A. Fisher, and N. Rostoker, Phys. Fluids **31**, 916 (1988).
[20] H. Ishizuka, G. Leslie, B. Mandelbaum, A. Fisher, and N. Rostoker, IEEE Trans. Nucl. Sci. **NS-32**, 2727 (1985).
[21] H. Ishizuka, J. Saul, A. Fisher, and N. Rostoker, in *Proceedings of the 6th International Conference on High-Power Particle Beams*, edited by C. Yamanaka (Institute of Laser Engineering, Osaka Univ., Osaka, Japan, 1986), p. 722.
[22] H. Ishizuka, R. Prohaska, A. Fisher, and N. Rostoker, in *Proceedings of the 7th International Conference on High-Power Particle Beams*, edited by W. Bauer and W. Schmidt (Kernforschungszentrum, Karlsruhe, Federal Republic of Germany, 1988), p. 857.
[23] H. Ishizuka, R. Prohaska, A. Fisher, and N. Rostoker, in *Proceedings of the 1989 IEEE Particle Accelerator Conference* (IEEE, New York, 1989), Vol. 1, p. 615.
[24] H. Ishizuka, A. Fisher, K. Kamada, R. Prohaska, and N. Rostoker, in *Proceedings of the 1987 IEEE Particle Accelerator Conference*, CH2387-9 (IEEE, New York, 1987), p. 136.
[25] D. Chernin, IEEE Trans. Nucl. Sci. **NS-32**, 2504 (1985).
[26] See AIP Document No. PAPS-PFBPE-02-3149-36 for 36 pages of "Orbital Resonances and Energy and Current Limits in High Current Cyclic Accelerators," SAIC Report No. SAIC-86/1516 by D. Chernin (1986). Order by PAPS number and journal reference from American Institute of Physics, Physics Auxiliary Publication Service, 335 East 45th Street, New York, NY 10017. The price is $1.50 for each microfiche (98 pages) or $5.00 for photocopies of up to 30 pages, and $0.15 for each additional page over 30 pages. Airmail additional. Make checks payable to the American Institute of Physics.
[27] See AIP Document No. PAPS-PFBPE-02-3149-116 for 116 pages of

"Modified Betatron Accelerator Studies," AMRC-R-655 by T. P. Hughes and B. B. Godfrey (1984). Order by PAPS number and journal reference from American Institute of Physics, Physics Auxiliary Publication Service, 335 East 45th Street, New York, NY 10017. The price is $1.50 for each microfiche (98 pages) or $5.00 for photocopies of up to 30 pages, and $0.15 for each additional page over 30 pages. Airmail additional. Make checks payable to American Institute of Physics.
[28] G. Roberts and N. Rostoker, Phys. Fluids **29**, 333 (1986).
[29] D. Chernin, Phys. Fluids **29**, 556 (1986).
[30] T. P. Hughes and B. B. Godfrey, Phys. Fluids **29**, 1698 (1986).
[31] See AIP Document No. PAPS-PFBPE-02-3149-98 for 98 pages of "Recirculating Accelerator Studies," AMRC-R-922 by T. P. Hughes and B. B. Godfrey (1987). Order by PAPS number and journal reference from American Institute of Physics, Physics Auxiliary Publication Service, 335 East 45th Street, New York, NY 10017. The price is $1.50 for each microfiche (98 pages) or $5.00 for photocopies of up to 30 pages, and $0.15 for each additional page over 30 pages. Airmail additional. Make checks payable to the American Institute of Physics.
[32] J. M. Peterson and J. B. Rechen, IEEE Trans. Nucl. Sci. **NS-20**, 790 (1973).
[33] H. Ishizuka, Y. Suzuki, and G. Miyamoto, Jpn. J. Appl. Phys. **4**, 1002 (1965).
[34] H. Dreicer, Phys. Rev. **115**, 238 (1959).
[35] D. J. Rose and M. Clark, Jr., *Plasmas and Controlled Fusion* (Wiley, New York, 1961).
[36] K. Len, J. Golden, T. Smith, D. Dialetis, S. J. Marsh, J. Mathew, P. Loshialpo, J. H. Chang, and C. A. Kapetanakos, Bull. Am. Phys. Soc. **34**, 1988 (1989).

Presented at BEAMS '88, Karlsruhe, Germany, July 4-8, 1988

SUPPRESSION OF BEAM INSTABILITIES IN THE UCI STELLATRON

H. Ishizuka, R. Prohaska, A. Fisher and N. Rostoker
Department of Physics, University of California
Irvine, California 92717, USA

Confinement of electron beams in a stellatron accelerator was studied. Experiments were conducted on beams of over 1 kA generated by means of plasma startup. Electron losses due to the orbital resonances were eliminated by improving the uniformity of the toroidal magnetic field. The negative mass instability caused serious disruption if the beam was distant from the torus wall. The betatron flux condition was controlled over time to keep the beam near the outer wall of the torus. Beam energies of up to several MeV were reached without significant loss of electrons. 1 kA 10 MeV beams were observed when 2 kA beams were initially formed and gradually decayed as the acceleration proceeded.

INTRODUCTION

The stellatron is a high current electron accelerator that employs a stellarator field for focusing and a betatron field for acceleration.[1] In an early stage of the experiment at UC Irvine, formation of a 200 A beam and acceleration up to 4 MeV were demonstrated using an electron injector.[2] Since then efforts have been made to increase the beam current and energy. Plasma startup in high vacuum led successfully to formation of a multi-kA beam of runaway electrons. The energy passed a target figure of 10 MeV, but the current dropped off during acceleration due to instabilities.[3] In this paper we study how to suppress the electron losses, placing the emphasis on beams of over 1 kA.

APPARATUS

The initial experimental setup was described in the previous papers.[2,3] Some modifications were made without changing the scale of the machine, and the present configuration is shown schematically in Fig. 1. A circuit to drive the betatron field coils is given schematically in Fig. 2.

Toroidal Field

Instead of 24 coils in the former system, 36 coils were equally spaced around the major axis of the machine to generate the toroidal magnetic field. The spatial ripple of the field on the axis of the torus was reduced to ± 0.1% from ± 2%. At the outer edge of the torus, the ripple was ± 8% in the old system but now it is less than ± 1%. This change was made to reduce the beam loss due to orbital resonances, which was observed in earlier experiments[2,3]

and also predicted theoretically.[4] The maximum field strength and the rise time are 17 kG and 120 μs, respectively.

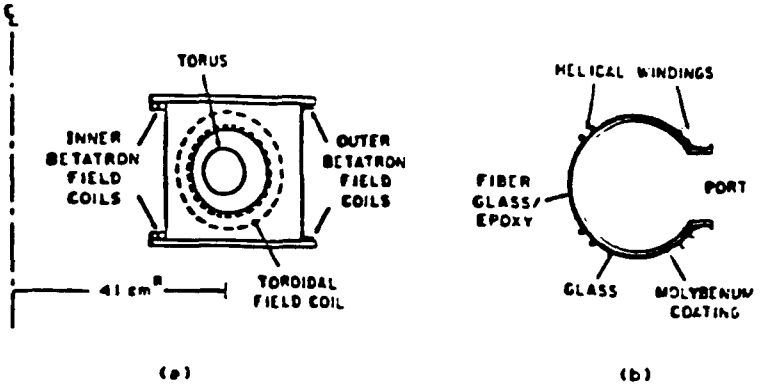

Fig. 1. (a) Schematic of the experimental setup. (b) Cross section of the torus with helical (rotating quadrupole) windings on it.

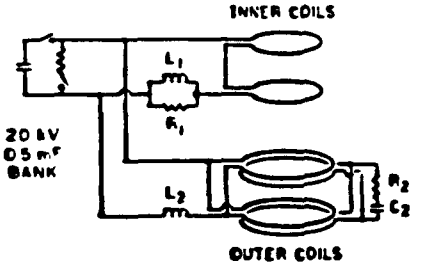

Fig. 2. Circuit to drive the betatron field coils.

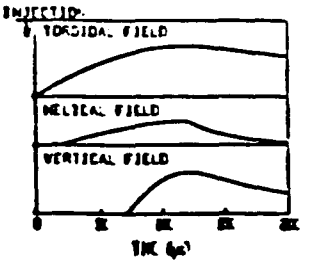

Fig. 3. Time sequence of operation.

Helical Field

The toroidal field was improved at the sacrifice of access to the inside of the coils. In a series of experiment, the azimuthal mode number m of the stellarator field was progressibely reduced from 12 down to 1. Lack of space between the toroidal field coils and vacuum chamber made it impossible to mount the helical windings inside the toroidal field coils as in the previous experiment.[2] New helical wires were wound directly on the torus (Fig. 1b). To mitigate the magnetic force, 8 wires were used instead of 4 and the current in the windings was cut off with a switch around the peak of the betatron field (Fig. 3).

Betatron Field

Initially the betatron field was produced by a pair of Helmholtz coils (two turns each) and a center solenoid (seven turns). In order to control the radial position of the beam during acceleration, a resistor was introduced in series with the center solenoid and in parallel with an inductor to manipulate the betatron condition. The beam current at 10 MeV was raised from 400 A to 800 A by this method. New coils as shown in Fig. 1 and the circuit in Fig. 2

were built to cover a wider range of orbit control. The upper and lower loops on the inner side were connected in series, and those on the outer side were connected in parallel. The resistor R_1 was changed within a range of 0.05-0.45 ohms at intervals of 0.05 ohms. L_1 and L_2 were altered within 1-4 μH. R_2 and C_2 were typically 0.5 ohms and 7.5 μF, respectively. The maximum field on the torus axis was 1 kG and the field rise time was 50-60 μs.

Torus

A torus made of graphite/epoxy composite was tried for several months. It was strong enough to stand the stress caused by the magnetic force exerted to the helical wires. It was also suited to attachment of a tangential port for beam extraction. However, the following drawbacks were observed: (i) the base pressure was not sufficiently low and (ii) the inner wall was damaged by beam bombardment. The current and the lifetime of the beam became worse with the lapse of time, and the graphite torus was finally given up. Thereafter a glass torus reinforced with glass fiber/epoxy composite (Fig. 1b) was used.

EXPERIMENT

Earlier Results

A small plasmoid was injected into a torus from a coaxial gun.[5] The plasma was confined in a rising stellarator field and expanded around the major diameter of the torus. A runaway electron current started when a betatron field was applied. The peak current reached a few kA, but electrons were lost as they were accelerated. The loss occurred in the following way: first, a steep descent of the beam current happened at 1-2 MeV. Second, the beam that had survived the first disruption decayed gradually. Finally, the beam current truncated when the ratio of the vertical field to the toroidal field reached a certain value. The first loss is attributed to the negative mass instability, and the second and third are explained by orbital resonances.[3]

An experiment was carried out on extraction of the beam out of the torus, and about 10% was removed into a tangential port.[6] In this connection, the mode number m of the stellarator field was scanned from 12 down to 1. Smaller m's gave better extraction efficiencies. The beam's life ended when $B_t/B_v \approx 24 - m$, where B_t and B_v are the toroidal and vertical fields, respectively.

New Results

1. Prolongation of Beam's Lifetime

The modified apparatus, in which m was 4, was operated in a similar manner. The time sequence of operation is shown in Fig. 3. The beam was generated using plasma startup, and the current was controlled by injection parameters to over 3 kA. The optimum rotational transform angle ι of the stellarator field was ≈ 0.1 with $\pm$ 30% tolerance at the start of the betatron field, consistent with

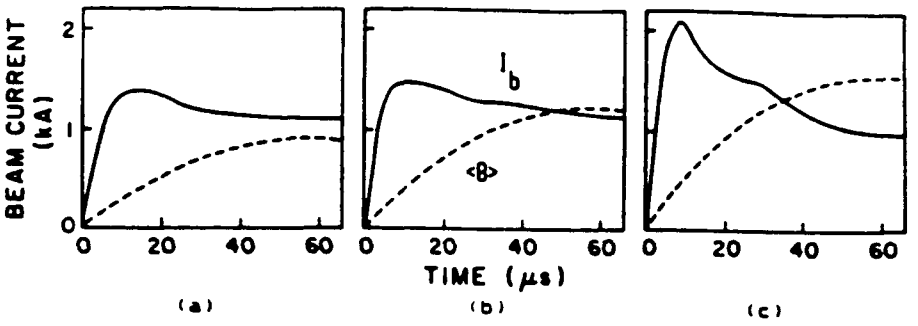

Fig. 4. Beam current (solid line) and betatron flux (dotted line). Peak beam energy: (a) 4 MeV, (b) 5.5 MeV, and (c) 7 MeV.

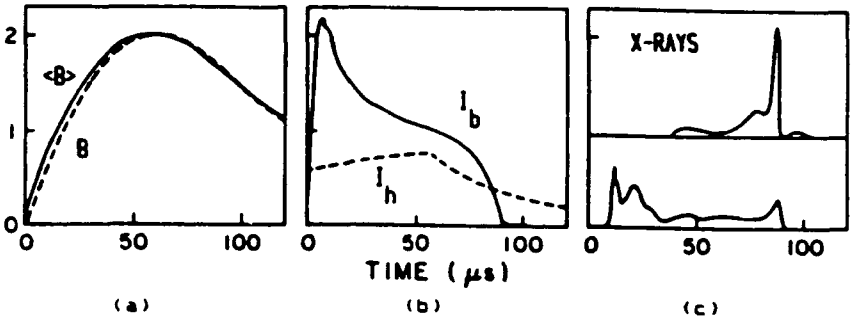

Fig. 5. Set of signals for a 10 MeV shot. (a) Betatron flux (solid line) and field (dotted line). (b) Beam current (solid line, in kA) and helical current (dotted line). (c) X-rays from a major source (upper) and plasma injector (lower).

the previous results. The beam's lifetime was clearly prolonged when the number of the toroidal field coils was increased to 36. The beam did not truncate as with 24 coils. A few hundred amperes easily passed the peak of the betatron field that corresponded to 10 MeV, and the termination occurred after the helical current was cut off.

2. Containment of High Current Beams

The disruption of high current beams in an early phase of acceleration was not cured but became even worse by improving the toroidal magnetic field. From the beginning of our stellatron experiment, the value of $\langle B \rangle / B$ was made larger than 2 to obtain a good beam.[5,7] Here B is the vertical magnetic field on the minor axis of the torus and $\langle B \rangle$ is the average inside. For high current beams, $\langle B \rangle / B > 2$ was definitely needed to avoid the beam disruption at 1-2 MeV. If $\langle B \rangle / B$ was too large, however, the beam could not stay long in the torus and the current decreased quickly in the rising betatron field. The control of $\langle B \rangle / B$ over time was tried for these reasons. The resistor R_1 shown in Fig. 2 advanced the phase of current flowing in the inner betatron field coils. $\langle B \rangle / B$ was large at the beginning and decreased with time.

The plasma source voltage was varied, while changing L_1, L_2 and R_1, to maximize the beam current at the peak of the betatron field. Figure 4 shows

examples of beam currents for different values of peak betatron field, obtained by varying the charging voltage. R_1 = 0.25 ohms in this series. The dotted lines show the loop voltages integrated over time, i.e. the magnetic flux inside the major radius of the torus. In Fig. 4a, where the peak electron energy was 4 MeV, the beam current is nearly constant after the initial broad peak. X-ray signals exhibited many small peaks successively during the peak of the beam current. Similar behavior of the beam but a slightly faster decay was seen when the peak beam energy was increased to 5.5 MeV (Fig. 4b). The decay was much more pronounced when the peak betatron field was further increased. A larger amount of plasma was injected to get the result shown in Fig. 4c. The beam current exceeded 2 kA and then decayed rapidly. Abrupt disruption happened if the injected plasma density was further increased, and the beam current after the disruption became smaller as the peak current was made larger.

A set of waveforms for R_2 = 0.45 ohms is given in Fig. 5. The vertical scale gives the beam current in kA. Other signals are in arbitrary units. The waveforms of magnetic flux (solid line) and the vertical field (dotted line) are compared in Fig. 5a. The beam current (solid line) and the helical current (dotted line) are shown in Fig. 5b. Here the beam current is 1 kA at 10 MeV and terminates after the helical current has fallen significantly. Figure 5c shows X-ray signals. The upper trace came from a PIN diode aimed at one of the spots where the major portion of the beam is lost. The lower one is a signal from a PIN diode looking at the plasma source, whose tip stuck into the torus by 1 mm from its outer wall. Actually the lower signal was smaller than the upper one by an order of magnitude. It is seen that X-rays were produced at the injector throughout the beam's life. The early disruption of the beam occurred if the experimental parameters were changed to delay the appearance of these X-rays.

Three comments are added as follows: (1) Metallic wires with different thicknesses (5 mil to 1 mm in diameter) were inserted into the torus for the purpose of controlling the electron loss, but the beam was not improved by this means. (2) Either additional plasma or electrons were injected after the start of acceleration for the purpose of increasing the energy spread of the beam, but the instability was not removed. (3) The beam current at several MeV was maximized to 2 kA by initially producing a beam of over 3 kA and properly increasing $\langle B \rangle / B$ to avoid the early disruption.

DISCUSSION

Stability of high current beams in a stellatron has been theoretically studied in detail. Three types of instabilities that would limit current and energy were emphasized: (1) orbital resonances, i.e. resonant excitation of betatron oscillations due to field and focusing errors,[1,4] (2) the negative

mass instability,[8,9] and (3) electromagnetic instability arising from a three wave interaction between the static helical field, a transverse mode on the beam, and a transverse-electric wave mode.[10] Evidently, the first two of them caused trouble in our stellatron.

Orbital Instability

In an ℓ=2 stellatron the betatron tune takes four values. Two of them, approximately given by $B_t/B_v + m$ and $-B_t/B_v$ in the limit of strong toroidal field, decrease quickly as B_v is increased. Our electrons thus see many integer and half-integer resonances during acceleration, as frequently as ~ 10 per μs. With the old system having 24 toroidal field coils, gradual decay and sharp termination of the beam were observed. That the beam ended when B_t/B_v became approximately 24 - m indicated that the resonance coupled with the bumpiness in the toroidal magnetic field was serious. After the bumpiness was reduced by an order of magnitude using 36 coils, the decay was suppressed and particularly the truncation of the beam vanished.

A strong toroidal magnetic field was necessary to confine a high current beam. It must have provided a well compressed plasma at the start of acceleration. At the same time it is required for minimizing resonant losses,[4] because the resonance is higher order and the tunes are less sensitive to the beam current the larger is the toroidal magnetic field.

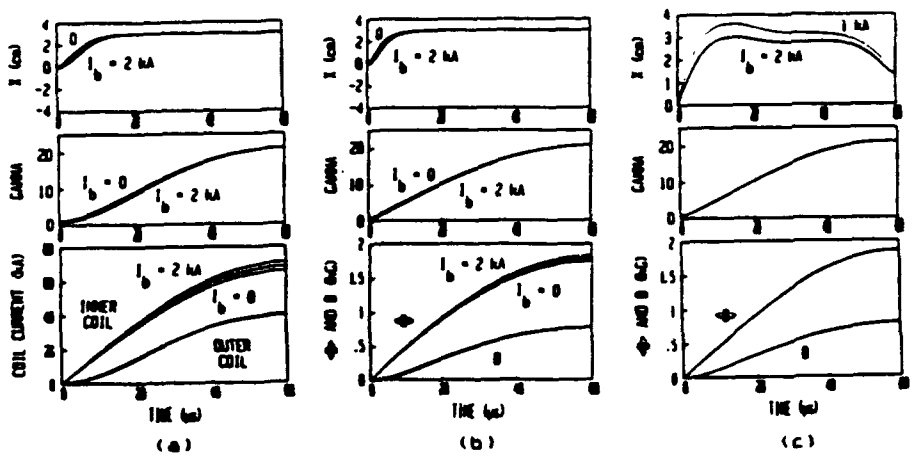

Fig. 6. (a) Betatron coil current to shift and keep the beam orbit near the outer torus wall. (b) Betatron flux and field. (c) Shift of beam position x for given ⟨B(t)⟩ and B(t).

Negative Mass Instability

The beam disruption at 1-2 MeV was attributed to the negative mass instability from the threshold energy at which it occurred and frequencies of RF generated. It was shown theoretically that background ions reduce the growth rate significantly,[11] yet the disruption was quite severe. As seen in the previous section, the abrupt loss was replaced by a gradual one.

The beam center in the stellatron is a helix around a circle, as confirmed experimentally.[6] Let us put the radius of this circle as R + x, where R is the major radius of the torus. The minor radius of the helix is about 0.16x for our case (m = 4, ι = 0.1, B_t = 15 kG). If we assume that the beam radius is 5 mm, the beam touches the torus wall when x ≈ 3 cm. In Fig. 6a, the currents in the betatron field coils for x to exponentially converge from 0 to 3 cm are calculated. The waveform for the inner coils was taken to be sinusoidal. The rate of the shift was so chosen that x becomes 2.7 cm at 1.5 MeV, a typical transition energy. <B> and B calculated under the same condition are shown in Fig. 6b. <B> assumes a sinusoidal waveform in this case. It is seen that <B>/B is large at the beginning: the beam is to be forced outwards and the flux change due to the increasing beam current must be compensated. <B>/B at the peak field is nearly 2.2 - 2.3 depending upon the beam current. The coil currents and the field strengths derived here are in close agreement with experimental values.

Figure 6c shows x(t) calculated for <B(t)> and B(t) as given at the bottom. It indicates that a beam stays at nearly the same average x-position while losing electrons. Experimental measurements and calculations show in detail how the beam position depends on the applied fields and the beam current.

No one has ever succeeded in stabilizing the negative mass instability by electronic feed-back. We have suppressed the disruptive loss of electrons by controlling the beam position, in which case there remains a small but continuous beam loss that involves skimming of the beam by the outer wall presumably because of the helical shape of the beam coming from a saturated kink mode. For a complete solution of the negative mass instability problem, novel schemes such as inductive walls should be considered.[12]

ACKNOWLEDGEMENT

This work was supported by the Office of Naval Research.

REFERENCES

1. C. W. Roberson, A. Mondelli and D. Chernin, Part. Accel. 17, 79 (1985).
2. B. Mandelbaum, H. Ishizuka, A. Fisher and N. Rostoker, Phys. Fluids 31, 916 (1988).
3. H. Ishizuka, J. Saul, A. Fisher and N. Rostoker, Proc. 6th Int. Conf. on High Power Particle Beams, 1986, edited by C. Yamanaka, p. 722.
4. D. Chernin, SAIC Report No. SAIC-86/1516 (1986).
5. H. Ishizuka, G. Leslie, B. Mandelbaum, A. Fisher and N. Rostoker, IEEE Trans. Nucl. Sci. NS-32, 2727 (1985).
6. H. Ishizuka, A. Fisher, K. Kamada, R. Prohaska and N. Rostoker, 87CH2387-9 (Proc. 1987 IEEE Particle Accelerator Conference) p. 136.
7. B. Mandelbaum, PhD. Dissertation, UC Irvine, 1985.
8. D. Chernin, Phys. Fluids 29, 556 (1986).
9. B. B. Godfrey and T. P. Hughes, Part. Accel. 21, 173 (1987).
10. T. P. Hughes and B. B. Godfrey, Phys. Fluids 29, 1698 (1986).
11. T. P. Hughes and B. B. Godfrey, AMRC-R-922 (1987).
12. R. J. Briggs and V. K. Neil, Plasma Physics 8, 255 (1966).

Presented at SPIE '91, Los Angeles, CA, January 21-24, 1991

A PLASMA BETATRON WITHOUT GAS BREAKDOWN

H. Ishizuka, K. Yee, A. Fisher and N. Rostoker

University of California, Irvine, California 92717 USA

1. ABSTRACT

Following Budker's proposal[1], experiments on plasma betatrons were carried out in several laboratories. Large conduction currents were observed as a result of gas breakdown, but the current of energetic electrons did not exceed 10 A. We adopted plasma injection to start a beam in good vacuum. The chamber consisted of outer and inner glass pipes lined with stainless steel mesh at radii of 5 cm and 2 cm, respectively. A toroidal field of 2 - 3 kG was applied along with a vertical field of up to 1.4 kG. Plasma was injected by coaxial guns, 1/4 inch in outer diameter, without increasing the neutral pressure significantly. A 20 A beam was accelerated to a peak energy of 1 MeV with little loss and then dumped to the chamber wall by a spiller field. The current was enhanced to more than 100 A by the addition of electron injection using a field emission cathode.

2. INTRODUCTION

The beam current in a conventional betatron is limited by the space charge at the injection time. The modified betatron[2,3] was proposed to focus an intense beam with the use of a toroidal magnetic field. However, it turned out that the beam's centroid is unstable during acceleration. The addition of a rotating quadrupole field[4] to the modified betatron is quite effective in improving the stability, as verified experimentally.[5,6]

The space charge limit can be eliminated if background ions exist. A stabilized, super-pinched beam was proposed by Budker[1], and experiments on the so-called plasma betatron were conducted in several laboratories. Large runaway currents were observed, but the current of energetic electrons did not exceed 10 A. Recently, beam currents of up to a few kA were generated in a stellatron by injecting plasma into a highly evacuated torus. In particular a 1 kA beam was accelerated to 10 MeV. Although the stellatron has been the only successful high-current betatron thus far, it has two disadvantages. One of them is

that the machine is rather complex in structure. The other is that the beam suffers orbital resonances during acceleration. These problems are less serious with modified betatrons.

In the UCI stellatron that used plasma startup, no beams were formed in the absence of the rotating quadrupole field. The aspect ratio of the apparatus in this case was approximately 10. One expects plasma electrons launched into a betatron orbit to tolerate, at the start of this acceleration, the mismatch between their momenta and the vertical field if the aspect ratio is reduced. This consideration motivated the present work. The theory of a plasma-assisted modified betatron[7] was taken into account. The subject is related to the runaway current in fusion devices, and also to the trapping and confinement of intense relativistic electron beams in a tokamak plasma.[8]

3. APPARATUS

A schematic of the apparatus is shown in Fig. 1. The vacuum chamber consisted of outer and inner glass pipes and end flanges. The outer pipe, 4.5" in diameter, had three ports: one for pumping, one for an electron injector, and another for plasma injectors and diagnostics. The inner pipe was 1.5" in outer diameter. The two pipes were lined with stainless steel screen. The system was evacuated down to 10^{-7} torr by a cryogenic pump.

The betatron field was produced by a pair of ten-turn coils. A pair of aluminum field-shapers were inserted between the coils and the vacuum chamber to minimize the field error due to current-feeds. The radial distribution of the field and the index are shown in Fig. 2. A center solenoid located inside the inner glass pipe produced the magnetic flux necessary for the betatron condition. The coils were energized by a 0.5 mF capacitor bank. A toroidal magnetic field was generated by wires stretched axially inside of the center solenoid. A 1 mF bank was used as the power supply. A rectangular coil (hereafter referred to as the spiller) was placed below the vacuum chamber. It was activated by a 0.8 μF, 15 kV capacitor; its purpose was to dump the beam at a preset time.

Plasmoids were injected by small plasma guns that stuck into the vacuum chamber through the end and top flanges. The electron injector was a field-emission cathode (either with or without an anode structure). A 100 ns negative voltage pulse of typically 40 kV was applied from a line-pulser to the cathode which caused an emission of up to 40 A. The machine was operated at about 0.5 pps for a peak beam energy of 0.5 MeV, and the repetition rate was reduced to 0.25 pps for a 1 MeV peak energy. Experiments were conducted within this range of peak energies, except when the machine was operated as a conventional betatron. The major parameters of the apparatus are given in Table I.

Table 1. Machine Parameters

Vacuum Chamber	
Type	Coaxial glass pipes lined with s.s. mesh
Outer radius	5 cm
Inner radius	2 cm
Vertical Field	
Peak (@ r = 3.5 cm)	3 kG
	1.4 kG rep-rated
Rise time	~ 200 μs
Toroidal Field	
Peak (@ r = 3.5 cm)	2 kG
Rise time	200-400 μs
Plasma Injector	
Type	Coaxial gun
Size	1/4" O.D.
Electron Injector	
Type	Field emission cathode
Voltage	40 kV typically

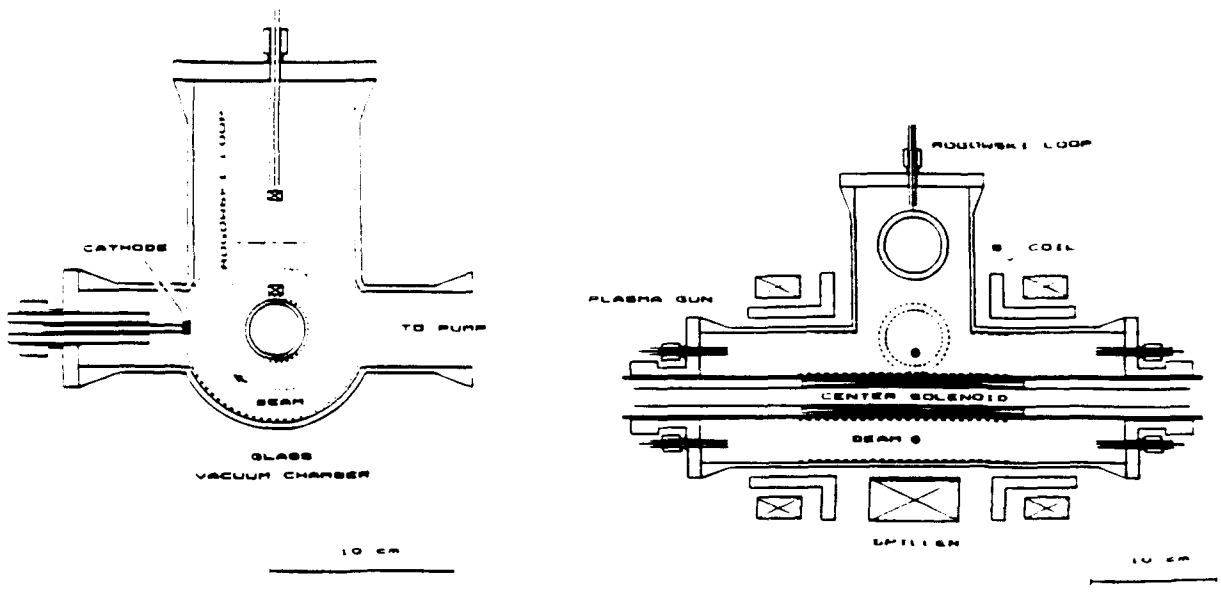

(a) (b)

Figure 1. Schematic of the experimental setup.

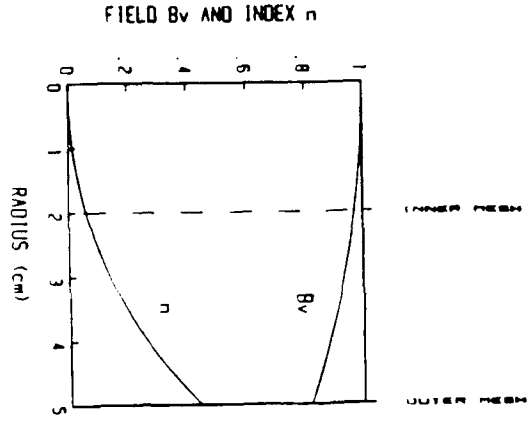

Figure 2. Radial distribution of the vertical field.

Note that the aspect ratio is as small as 2.3.

Diagnostics included PIN diodes, a plastic scintillator and a pin-hole camera for X-ray measurement. The plastic scintillator was encased in a lead shield with a 3 mm diam. hole in the front wall which was 125 cm away from the vacuum chamber. A Rogowski loop was

placed in the vacuum chamber due to a lack of space outside. To minimize the perturbation to the beam, the loop was kept high inside the top port (Fig. 1b) except when the measurement of the beam current was intended.

4. EXPERIMENTAL RESULTS

4.1 Operation as a Classical Betatron

The apparatus was initially operated as a classical betatron to test the betatron field. The electron injector consisted of a field emission cathode and anode. The toroidal magnetic field was not applied at this time. Accelerated beams were dumped to the chamber wall by applying the spiller field at the peak of the betatron field. No X-rays were detected between the injection and spill times (Fig. 3). In the single shot mode of operation, the peak betatron field was up to 3 kG at a radius of 3.5 cm, corresponding to an electron energy of 2.5 MeV. The rate of field rise in the initial phase was decreased to observe beams when the peak field was higher than 1 kG (Fig. 3b). A rapid rise of the field was unfavorable for beam formation possibly because of transient field errors and also due to a narrow window in time for injection.

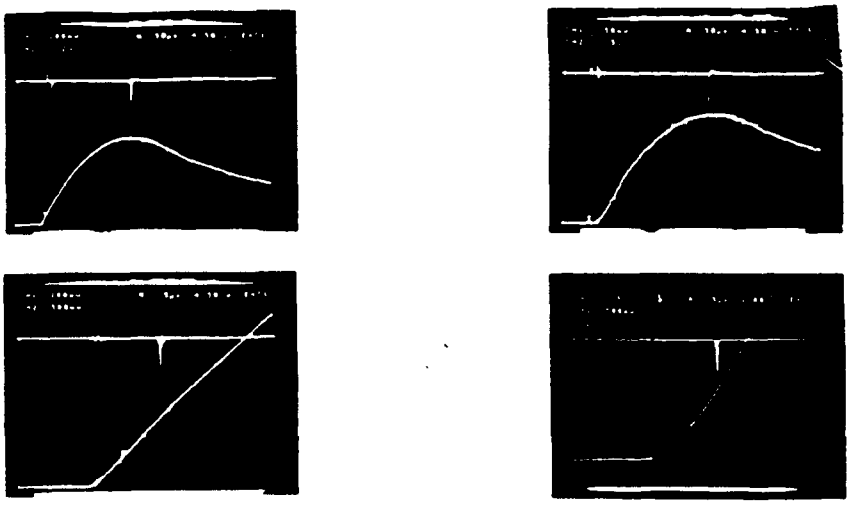

(a) (b)

Figure 3. Operation as a classical betatron. The peak electron energy is (a) 0.5 MeV and (b) 2 MeV. Sweep: 50 μs/div.

4.2 Plasma Anode

The beam was not observed if the anode was removed from the electron injector. However, the beam was recovered by firing a plasma gun in such a manner that the plasma ions were present around the field emission cathode at the injection time. Figure 4a shows the current in the plasma gun and an ion signal from a Langmuir probe placed close to the field emission cathode. Figure 4b shows the range of times of electron injection relative to plasma injection for the beam formation to occur. It is seen that the ion density should be a few times 10^{10} cm^{-3} or higher to observe a beam.

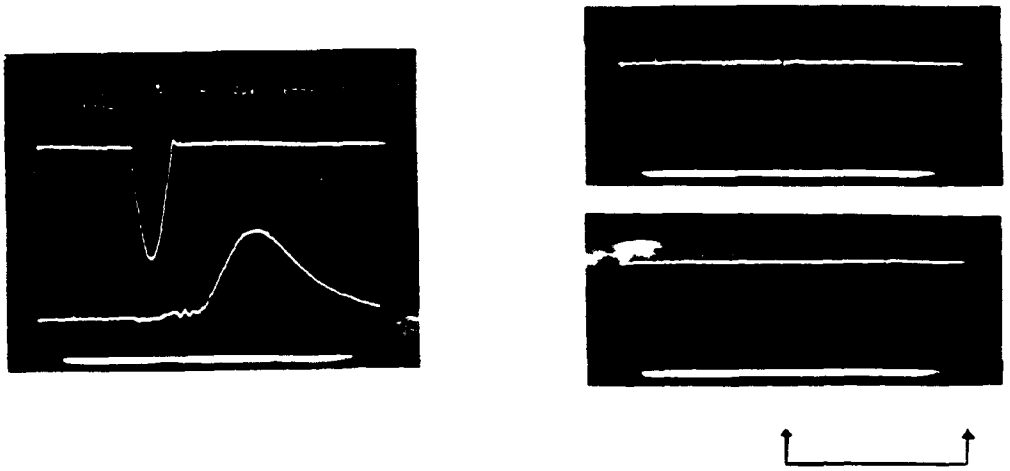

(a) (b)

Figure 4. Plasma anode. (a) Upper trace: plasma current. Lower trace: ion saturation current into a Langmuir probe near the field emission cathode. Ion density ~ 10^{11}/cc/div. (b) Electron injection pulse and the range of injection timing for the beam formation to occur. 2 μs/div.

4.3 Plasma Startup

Beams were accelerated from plasma (i.e. without operating the electron injector) in the modified betatron field. The toroidal magnetic field was switched on before the betatron field (Fig. 5a), which was adjusted to maximize the X-ray intensity at the spill time.

Plasma was injected at the start of the betatron field (Fig. 5b). The beam formation was fairly insensitive to the time of injection relative to the start of the betatron field. However, the highest X-ray intensity was obtained when the plasma gun was fired shortly before the start of the vertical field (Fig. 5b). Whether the betatron field waveform was sinusoidal or modified to reduce the rise rate did not influence the result. The X-ray intensity was much higher than in cases 4.1 and 4.2 mentioned above. Small bursts of X-rays were observed at times when the ratio of the vertical field to the toroidal field took certain values in the course of acceleration.

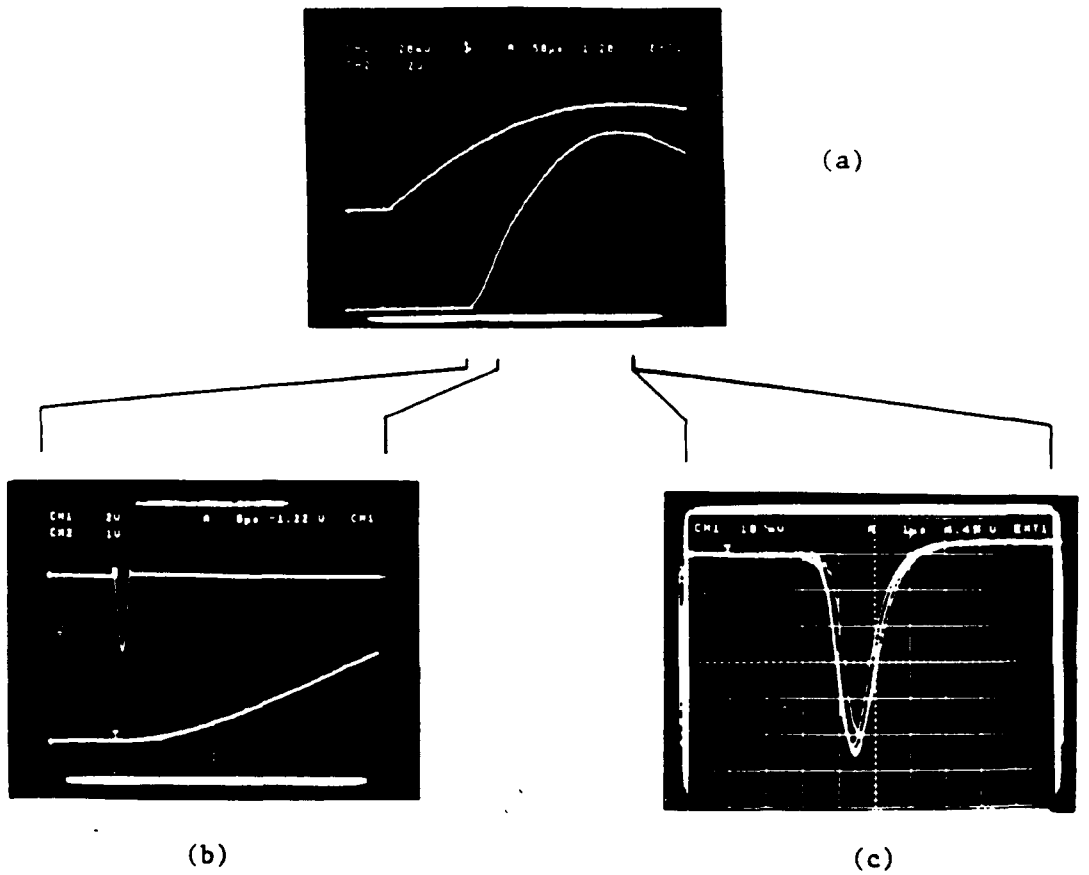

Figure 5. Plasma startup. (a) Upper trace: toroidal magnetic field. Lower trace: vertical field. 50 μs/div. (b) Upper trace: Plasma gun current. Lower trace: vertical field 5 μs/div. (c) X-ray signals due to the beams spilled at the peak field 1 μs/div.

The largest X-ray signal was observed when the flux condition was met at around a radius of 3.5 cm (i.e. middle of the two glass pipes). However, because of the small value of the aspect ratio smaller beams were accelerated even if the ratio of the current in the center solenoid to that in the field coil was varied significantly. Normally, two plasma guns were used simultaneously to insure symmetry with respect to the median plane. Various arrangements of plasma guns were tried. The maximum X-ray intensity was nearly independent of the gun location after optimizing other experimental parameters. Reduction of the X-ray intensity occurred when either a plasma gun was extended axially to within 3 cm of the median plane or when a gun from the top flange protruded beyond a radius of 5 cm as measured from the machine axis.

4.4 Current Enhancement by the Addition of Electron Injection

The beam intensity was enhanced drastically by adding electron injection to case 4.3 above. The electron injector was used as a field emission cathode, and the stainless steel screen liner served as the anode. Figure 6a shows optimum timings of the plasma injection and electron injection (upper trace) relative to the vertical field (lower trace). X-ray signals were observed from a beam started from plasma, and were intensified severalfold when the electron injector was operated. The X-ray intensity was sensitive to the timings of both plasma injection and electron injection. It was also sensitive to the position of the field-emission cathode (the cathode had to be nearly flush with, but slightly inside, the screen liner).

It was found that there is another set of timings that brings about a peak X-ray yield. In this case plasmoids were injected vertically close to the median plane, and electrons were injected only a few microseconds later (Fig. 6b). The X-ray intensity was very weak without the electron injection, but increased by orders of magnitude to the same level as in the case of Fig. 6a when electrons were injected. Note that the vertical field at the time of electron injection is significantly lower than in the conventional betatron mode (Fig. 3).

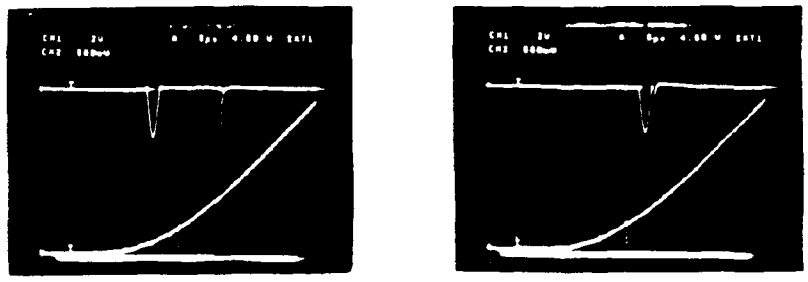

Figure 6. Timings of plasma and electron injections for producing the largest beam current. Upper traces: plasma gun current and electron injection pulse. Lower traces: vertical field. 5 μs/div.

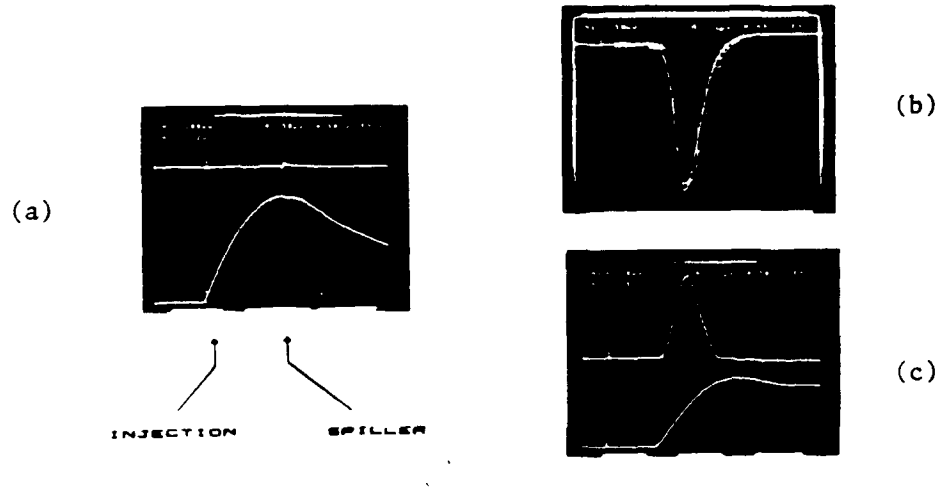

Figure 7. Spiller field and X-ray signals. (a) Time sequence. 50 μs/div. (b) Plastic scintillator output. 1 μs/div. (c) Upper trace: PIN diode output. Lower trace: current in the spiller coil. 1 μs/div.

The beam was dumped onto the screen liner at around the time of the peak of the vertical field. X-ray signals and the spiller current are shown in Fig. 7. The spiller field opposed the vertical field and dumped the beam within a few microseconds. (When reversing the field, a higher spiller current was necessary to totally dump the beam.) The beam orbit expanded due to the spiller and hit the outer wall, as indicated by X-ray pinhole pictures (Fig. 8). An X-ray pinhole camera was placed approximately 30 cm from the vacuum chamber, making an oblique angle to the median plane. With the aid of an intensifier, 50 to 100 irradiations gave a clear picture on a Polaroid film 107C (ASA 3000), when dumping 0.75 MeV beams. In Figure 8a (taken with a 3 mm diam. aperture) the elliptical ring corresponds to the outer screen liner on the median plane. Figure 8b, taken with a 1 mm aperture under a separate experimental condition, shows that the screen liner was bombarded by electrons at small spots. The location of the X-ray source was sensitive to perturbations of the toroidal magnetic field: the beam was dumped to one spot by properly tilting the spiller coil with respect to the median plane. (This will be favorable when beam extraction is attempted).

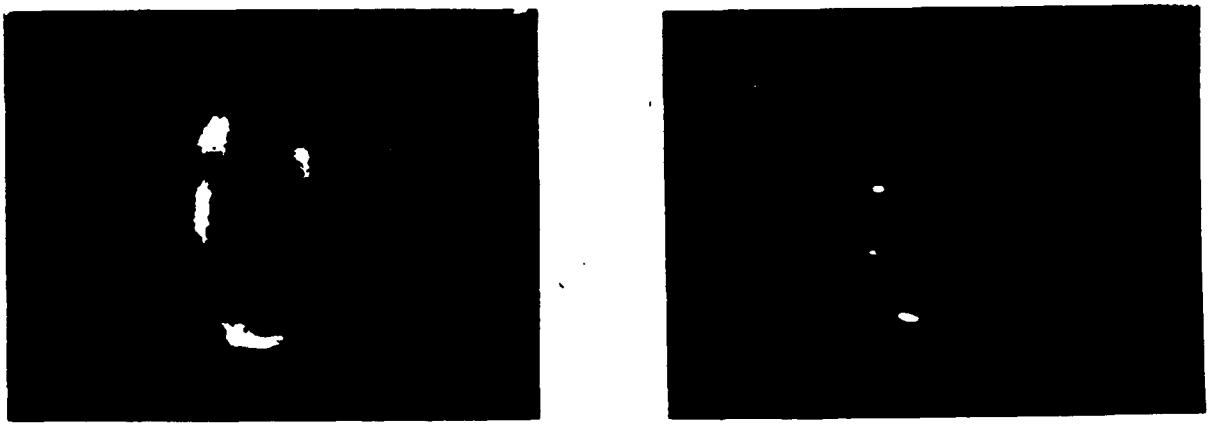

Figure 8. X-ray pinhole pictures. The aperture is (a) 3 mm and (b) 1 mm in diameter.

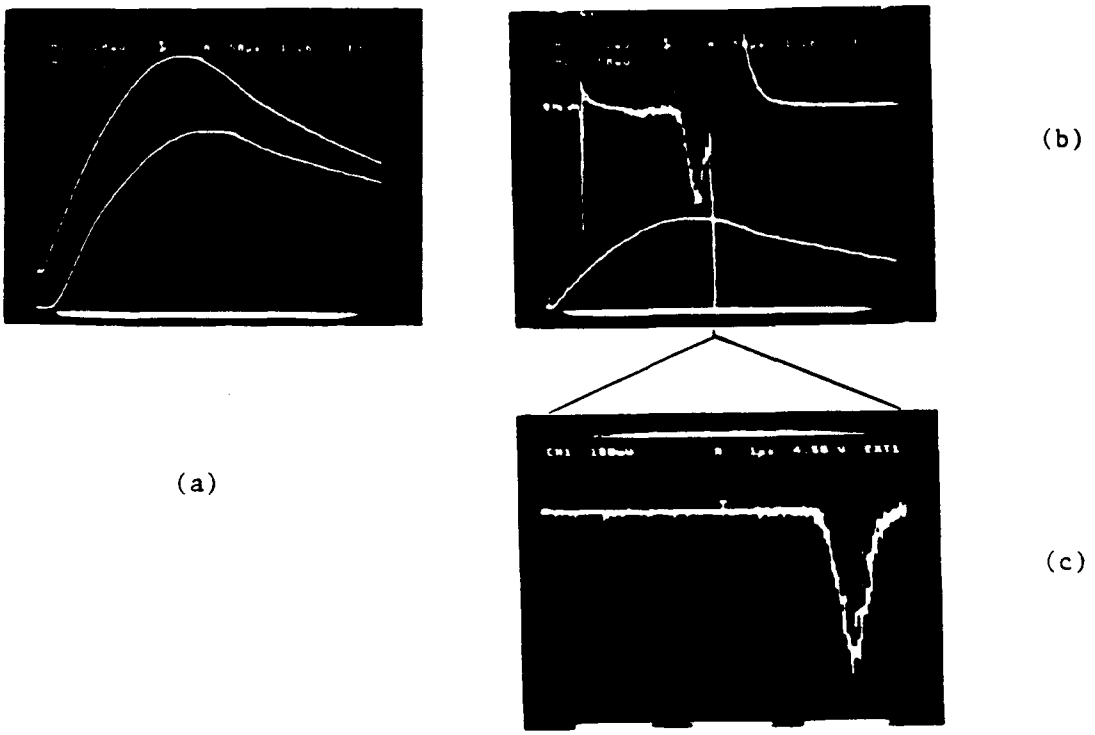

(a)

(b)

(c)

Figure 9. Loss of electrons. (a) Upper trace: toroidal magnetic field. Lower trace: vertical field. 50 μs/div. (b) Upper trace: X-ray signal. Lower trace: toroidal field. 50 μs/div. (c) X-ray signal at around the time when the beam is spilled. 1 μs/div.

Small beam losses were observed through X-ray emission during acceleration. The losses occurred in a similar manner as in (c). In Fig. 9b, in addition to a large peak due to the spiller applied at 240 microseconds, X-ray bursts were seen around 50 microseconds and 220 microseconds from the start of the toroidal magnetic field. A fast picture of the X-ray signal around the spill time is shown in Fig. 9c. In this case, the output of the photomultiplier tube was led directly (i.e. without an emitter follower) to a scope and terminated there by

a 50 ohm resistor. Single photons are seen before the major pulse. In order to estimate the accelerated charge, the X-ray detector system was calibrated using radioactive isotopes. Assuming that the angular distribution of the bremsstrahlung was isotropic, the accelerated charge was estimated to be 80 nC, giving a beam current of 110 A.

Measurements of the beam current were attempted by using a Rogowski loop. However, the perturbation to the beam was so large that the X-ray signal was reduced by an order of magnitude when the loop was inserted. Figure 10 shows currents measured by the Rogowski loop.

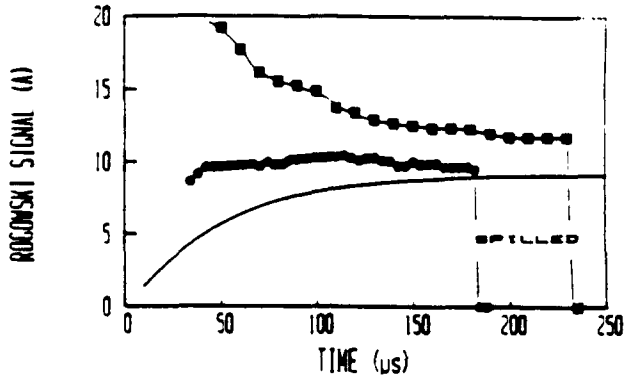

Figure 10. Current measured by a Rogowski coil. The X-ray intensity is reduced by an order of magnitude by the presence of the loop. The solid line shows the electron velocity (10 x v/c) evaluated from the betatron field.

The early part (< 30 microseconds from the start of the betatron field) of the Rogowski signal was masked by the noise coming from the field, plasma gun and electron injection pulse. The current appeared either flat or as a decreasing function of time. The solid line in the figure shows the temporal change of electron speed due to betatron acceleration. The difference in waveform between the current and the electron speed indicates the presence of a conduction current which decays with time. The X-ray signal was proportional to the current when the beam was spilled near the peak of the betatron field. This means that the

beam current dominates after acceleration. Currents up to 12 A were observed with the Rogowski loop. This corresponds to a beam current greater than 100 A, since the X-ray intensity is larger by an order of magnitude in the absence of the Rogowski loop. This is consistent with the estimate based on the X-ray field.

5. DISCUSSION

Beams were started from plasma in a modified betatron field. A toroidal magnetic field was definitely necessary to launch plasma electrons into the betatron orbit. From relative intensities of X-rays the beam currents were estimated as shown in Table II.

Table II. Beam Current in Different Modes

Classical betatron mode	Up to 0.4 A
Plasma anode	0.6 A
Plasma startup	20 A
Current enhancement with electron injection	110 A

Incidentally, the space-charge limit in the conventional betatron mode is 2.9 A/cm^2 under our experimental conditions.

Small beam losses occurred in the course of acceleration in the modified betatron field. Betatron tunes of a charge-neutralized beam depend upon the ratio of the toroidal magnetic field to the vertical field (and also on the current density). When this ratio decreases with time, as in our experiment, one of the betatron tunes takes on a large number at the initial stage of acceleration and subsequently decreases. The observed beam loss can be qualitatively attribed to low-mode integer resonances.

7. ACKNOWLEDGEMENT

This work was supported by the Office of Naval Research.

8. REFERENCES

1] Budker, G. I., Proc. in Proceedings of CERN Symposium on High Energy Accelerators and Pion Physics, Geneva 1956 (CERN Scientific Information Service, Geneva, 1956) Vol. 1, p. 68.

2] Rostoker, N., Particle Accelerators 5, 93 (1973).

3] Sprangle, P. and Kapetanakos, C. A., J. Appl. Phys. 49, 1 (1978).

4] Roberson, C. W., Mondelli, A. and Chernin, D., Particle Accelerators 17, 79 (1985).

5] Mandelbaum, B., Ishizuka, H., Fisher, A. and Rostoker, N., Phys. Fluids 31, 916 (1988).

6] Len, L. K., Golden, J., Smith, T., Dialetis, D., Marsh, S. J., Mathew, J., Loshialpo, P., Chang, J. H. and Kapetanakos, C. A., Bull. Am. Phys. Soc. 34, 1988 (1989).

7] Manheimer, W. M., Particle Accelerators 17, 157 (1985).

8] Mohri, A. Nucl. Fusion 25, 1299 (1985).

Presented at 1987 IEEE Particle Accelerator Conf., Washington, DC, 1987

PRELIMINARY EXPERIMENT ON THE ELECTRON BEAM EXTRACTION FROM A STELLATRON

H. Ishizuka, A. Fisher, K. Kamada, R. Prohaska and N. Rostoker
Physics Department
University of California
Irvine, California 92717

Abstract

The stellatron is a high current electron accelerator that employs a stellarator field in addition to the betatron field. A substantial fraction of 1 kA was accelerated to 10 Mev in a glass torus either lined with stainless steel mesh or coated with molybdenum. The same current and energy were observed with a torus made of graphite epoxy composite, to which an extraction port was attacned. A Faraday cup placed in this port detected electrons, up to 1 uC per pulse at beam energies of a few MeV, when a pulsed magnetic field was applied to expand the beam orbit.

Introduction

An experimental study of the stellatron has been pursued in the last three years. The goal (1 kA, 10 MeV) has been attained in regard to the electron current and energy but not simultaneously [1, 2]. The major issues to be addressed at this point are (1) suppression of beam decay and (2) extraction to facilitate emittance measurement and beam utilization in the absence of magnetic fields.

Method of Extraction

Problems

Several methods are applied to extract beams from conventional betatrons. The basic requirements for good extraction are (1) sufficient perturbation to permit electrons to jump out of the guiding field, (2) negligibly small influence on the beam before the extraction, and (3) focusing action. These are common to the stellatron case, while the field configuration and the beam dynamics are remarkably different. In the stellatron, electrons are much more reluctant to change their orbit. They do not move on planes. The stellarator field, which is stronger than the betatron field, increases toward the torus wall. Thus a new extraction scheme and/or modification of machine parameters are required.

Orbit Expansion

The closed orbit in a stellatron is a helix when there is mismatch between the electron momentum and the vertical field [3]. The beam center undergoes an oscillation around this closed orbit and electrons oscillate around the beam center. Let us consider a loop, indicated as the spiller in Fig. 1, that goes all the way around the major diameter of the torus. When a current is started in it to produce a field that opposes the betatron field, the closed orbit is driven outwards. The spiller field increases with radius, and the momentum compaction factor is greatly increased at a certain distance from the spiller winding. The beam orbit is expected to expand rapidly near this radial position.

Focusing

A drift space for extraction must be provided. A hollow conductor was used to screen the betatron and the helical fields. The toroidal field must extend into it to avoid electron deflection near the entrance.

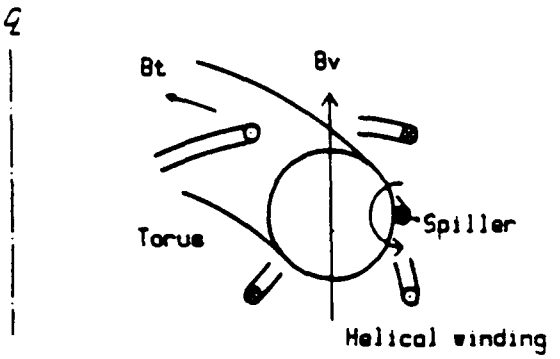

Fig. 1 - Spiller winding for orbit expansion.

The azimuthal mode number m of the stellarator field must be made as small as possible in order to reduce spirality of the orbit.

Experimental Procedure

The UCI stellatron has been operated at m = 12 or 8. The first step in this work was to operate the machine at a smaller m. The orbit expansion due to the spiller field was next verified using a Faraday cup inserted into the torus. The effect of field perturbations, that were caused by introducing a conductor into the torus, on the beam confinement was also examined. The beam energy was checked by placing absorbers in front of the Faraday cup. Then a half section of the glass torus was replaced by a graphite torus. An extraction port was attached and electrons were detected in it. The spiller was operated when the beam energy reached a few MeV.

Experiment

Apparatus

The vacuum chamber was 41 cm and 4 cm in major and minor radii, respectively. Three sets of magnetic fields were applied: the betatron field, toroidal field and the helical field [1]. In this series of experiment, the peak toroidal and the betatron fields were limited to 10.5 kG and 540 G, respectively, to facilitate machine maintenance. The spiller field was generated by discharging a 0.1 - 0.8 uF capacitor bank through a triggered sparkgap. The operating voltage was 20 - 40 kV.

Figure 2(a) shows a Faraday cup encased in a copper tube. The tube was typically 16 mm in outer diameter, 2.5 mm in wall thickness, and 40 mm in length. An aluminum filter (a disk used for electron absorption) covered the front end, while the rear end was shielded with copper. The Faraday cup was radially movable and also rotatable around a rigid coaxial cable. An extraction port attached to the graphite

torus is illustrated in Fig. 2(b). A copper snout, 19 mm in outer diameter and 3 mm in wall thickness, stuck into the torus. It was slotted so that the toroidal magnetic field penetrated.

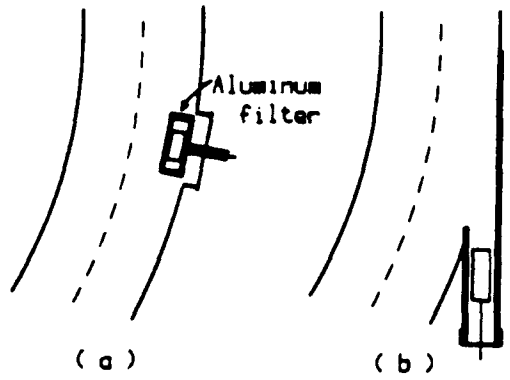

Fig. 2 - (a) Faraday cup inside the torus.
(b) Extraction port.

General Features

Typical time sequence of operation and signals are shown in Fig. 3. A plasmoid was injected into the torus, from either the outer or inner side, with a small plasma gun [2]. The plasma was confined by the stellarator field and a runaway current started when the betatron field was applied. The current was terminated by activating the spiller. At the same time, the Faraday cup and X-ray pin diodes presented signals which were as narrow as 200-300 ns. Dotted lines in the figure show the signals in the absence of the spiller field.

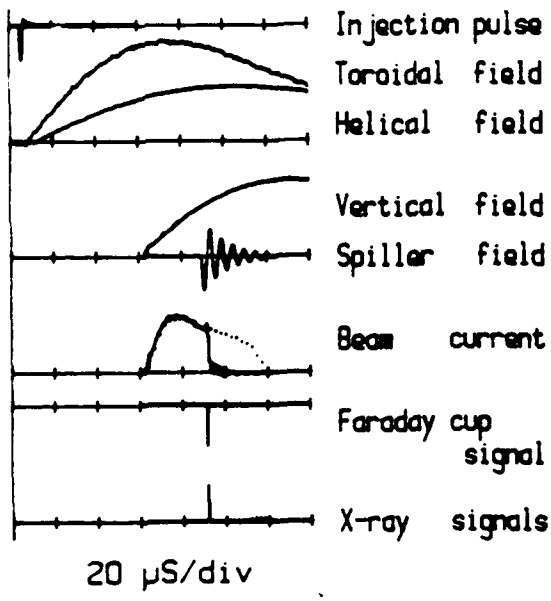

Fig. 3 - Typical time sequence of operation and signals.

Reduction of the Mode Number m

The helical windings were supported by 9-10 rings that fitted into the toroidal field coils. The pitch of the windings was constant within the rings but adjusted between the toroidal field coils to alter m. As a result, the windings deviated materially from pure helices for low values of m. Such a distortion has, however, little effect on the rotational transform angle [4]. As m was changed from 12 to 8, 6 and 4, the helical current necessary to observe the beam decreased. This critical current and the rotational transform angle are shown in Fig. 4. The beam current was insensitive to m, while the X-ray pin-hole

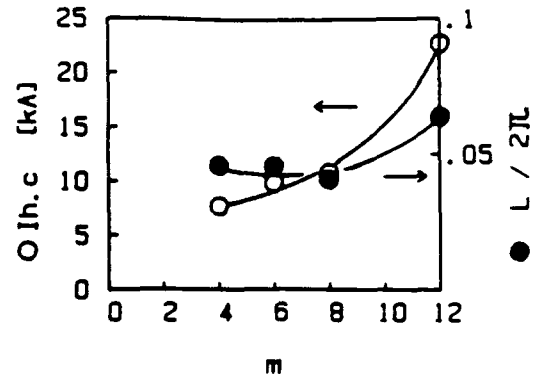

Fig. 4 - Critical helical current and rotational transform angle

pictures indicated that the axial pitch of the electron beam became longer with decreasing m as expected.

Faraday Cup Inside the Torus

The beam was not affected significantly if the far side of the copper tube stayed within approximately 1 cm from the outer wall of the torus. As it was moved inwards, the beam current decreased and the decay became quicker. The Faraday cup showed a signal when the spiller field was applied. The signal was largest when the Faraday cup was near and parallel to a helical wire which carried a current such that it repelled the beam. The peak reached 2 A and the half width was typically 100 ns. If the front disk was removed and the Faraday cup was rotated by 180 degrees, an ion signal appeared which was smaller than the said electron signal by two orders of magnitude. X-ray pinhole pictures showed that most of the beam electrons hit the copper tube.

The electron energy was evaluated by the absorption method changing the thickness of the aluminum disk. In Fig. 5 are plotted Faraday cup signals for three values of disk thickness against the time when the spiller field was applied. The solid lines are theoretical curves based on the electron transmission factor through slabs [5] and the betatron acceleration. The electron energy calculated from the betatron acceleration is also shown on the horizontal axis.

Removal out of the Torus

The beam current and the beam's behavior remained unchanged when replacing a half of the glass torus with a graphite torus. The snout was inserted within a limit not to disturb the beam, and the Faraday was placed so that its innermost edge stayed

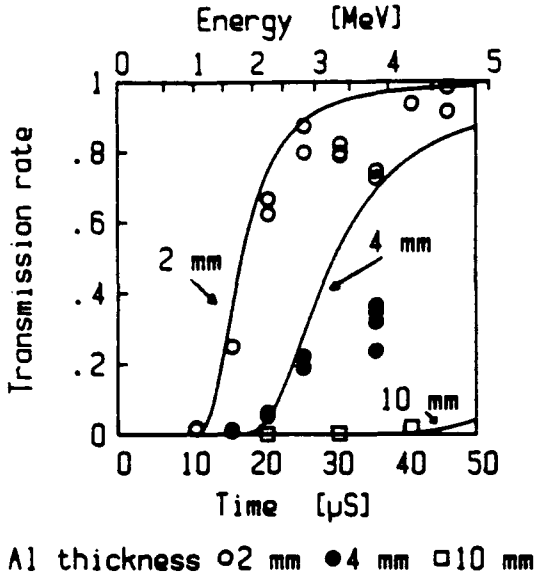

Fig. 5 - Electron transmission through aluminum disks.

inside the torus wall. A signal was obtained by applying the spiller field, as shown in Fig. 6, if the

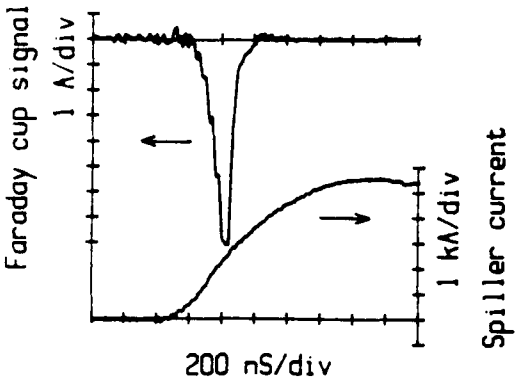

Fig. 6 - Electron removal into the extraction port

helical current nearest to the extraction port was in such a direction as to repel the beam. The signal was not affected by biasing the Faraday cup within ± 2 kV..

The collector current increased by a factor of 7 when m was reduced from 6 to 4. It increased with the operating voltage of the spiller. The peak signal and the collected charge reached 8 A and 1 μC, respectively. The signal started to rise when the spiller current was approximately 600 A and reached the peak at 1.6 - 2.4 kA. X-ray pin-hole pictures showed that most of the beam electrons hit the snout along the helical winding. If the Faraday cup was removed and the extraction port was vacuum-sealed at its end, electrons ejected into the air were observed visually with a plastic scintillator.

Discussion

We have observed for the first time extraction across the guiding fields in a stellatron. The beam orbit expands due to the spiller field and forms a helix corresponding to a theoretical closed orbit. About 10% of the beam enters a field excluding snout and is collected on an 11 mm diam Faraday cup. The rest of the beam hits the snout under the present conditions. The absorption data taken suggest that the electron energy is consistent with the betatron acceleration. For sake of comparison, we may observe that among conventional betatrons extraction efficiencies vary from 10% to 70% [6]. Azimuthally local field perturbations (coils or extraction snout) have little effect on stellatron performance. Another important finding is that the beam parameters are insensitive to the mode number m of the helical field. m will be reduced below 4 and the spiller will be operated at higher voltages in future to improve the extraction efficiency.

This work was supported by the Office of Naval Research.

References

[1] H. Ishizuka et al, "Injection and Capture of Electrons in the UCI Stellatron," Trans. Nucl. Sci., Vol. NS-32, No. 5, pp. 2727-2729, 1985.

[2] H. Ishizuka et al, "Beam Acceleration in the UCI Stellatron," in 6th Int. Conf. on High-Power Particle Beams, 1986 (to be published).

[3] C. W. Roberson, M. Mondelli and D. Chernin, "The Stellatron Accelerator," Particle Accelerators, Vol. 17, pp. 79-107, 1985.

[4] I. S. Danilkin, "Effect of Geometric Errors in the Magnetic System on the Field Configuration in a Stellarator," in Proc. of P. N. Lebedev Physics Institute, Vol. 65, 1979, pp. 23-45.

[5] C. D. Zerby and F. L. Keller, "Electron Transport Theory, Calculations, and Experiments," Nucl. Sci. Eng., Vol. 27, pp. 190-218, 1967.

[6] R. S. Foote and B. Petree, "A Pulsed Magnetic Extractor for Removing the Electron Beam from a Betatron," Rev. Sci. Instr., Vol. 25, pp. 694-698, 1954.